



Post-processing the National Water Model with Long Short-Term Memory Networks for Streamflow Predictions and Model Diagnostics

Journal:	<i>Journal of the American Water Resources Association</i>
Manuscript ID	JAWRA-20-0099-P.R2
Manuscript Type:	Technical Paper
Date Submitted by the Author:	n/a
Complete List of Authors:	Frame, Jonathan; University of Alabama, Geological Sciences Kratzert, Frederik; Johannes Kepler University, LIT AI Lab & Institute for Machine Learning Raney, Austin; University of Alabama, Geography Rahman, Mashrekur; University of California Davis, Department of Land, Air and Water Resources Salas, Fernando R.; NOAA, NWS Office of Water Prediction Nearing, Grey; Google Research
Category Headings:	HYDROLOGY, MODELING
Key Terms:	streamflow < HYDROLOGY, National Water Model, long short-term memory, post-processing, machine learning

1
2
3 1 Post-processing the National Water Model with Long Short-Term Memory Networks for Streamflow
4
5 2 Predictions and Model Diagnostics

6 3 Jonathan M. Frame, Frederik Kratzert, Austin Raney, Mashrekur Rahman, Fernando Salas and Grey S.
7
8 4 Nearing

9
10 5 Department of Geological Sciences, University of Alabama, Tuscaloosa, AL USA (Frame); LIT AI Lab
11 6 and Institute for Machine Learning, Johannes Kepler University, Linz, Austria (Kratzert); Department of
12 7 Geography, University of Alabama; Tuscaloosa, AL USA (Raney); Department of Land, Air and Water
13 8 Resources, University of California, Davis (Rahman); NOAA National Water Center (Salas); Google
14 9 Research, Mountain View, CA USA (Nearing).

15
16 9 (Correspondence to Frame: jmframe@crimson.ua.edu)

17
18
19 11 **Research Impact Statement:** Long Short-Term Memory (LSTM) models improve upon daily
20 12 streamflow predictions by the U.S. National Water Model (NWM). Including NWM model output as
21 13 input to the LSTM (i.e., post-processing) does not provide additional predictive performance. We
22 14 additionally used post-processing for diagnosing sources of error in the NWM and identified the NWM
23 15 channel router as a major source of information loss.

24
25
26
27 16 **ABSTRACT:** We build three Long Short-Term Memory (LSTM) daily streamflow prediction models
28 17 (deep learning networks) for 531 basins across the contiguous United States (CONUS), and compare their
29 18 performance: (1) a LSTM post-processor trained on the U.S. National Water Model (NWM) outputs
30 19 (LSTM_PP) as a target variable, (2) a LSTM post-processor trained on the NWM outputs and using
31 20 atmospheric forcings (LSTM_PPA), and (3) a LSTM model trained on USGS average daily streamflow
32 21 data and using atmospheric forcing (LSTM_A). We trained the LSTMs for the period 2004-2014 and
33 22 evaluated on 1994-2002, and compared several performance metrics to the NWM reanalysis. Overall
34 23 performance of the three LSTMs is similar, with median NSE scores of 0.73 (LSTM_PP), 0.75
35 24 (LSTM_PPA), and 0.74 (LSTM_A), and all three LSTMs outperform the NWM validation scores of 0.62.
36 25 Additionally, LSTM_A outperforms LSTM_PP and LSTM_PPA in ungauged basins. While LSTM as a
37 26 post-processor improves NWM predictions substantially, we achieved comparable performance with the
38 27 LSTM trained without the NWM outputs (LSTM_A). Finally, we performed a sensitivity analysis to
39 28 diagnose the land surface component of the NWM as the source of mass bias error and the channel router
40 29 as a source of simulation timing error. This indicates that the NWM routing scheme should be considered
41 30 a priority for NWM improvement.

42 31 **(KEYWORDS:** National Water Model; theory-guided machine learning; long short-term memory;
43 32 streamflow; model diagnostics.)
44
45
46
47
48
49
50
51
52
53
54
55
56
57
58
59
60

33 INTRODUCTION

34 The U.S. National Water Model (NWM), based on WRF-Hydro (Cosgrove *et al.*, 2015),
35 is an emerging large-scale hydrology simulator. Some specific details of the NWM
36 advancements in large scale hydrology are described by Elmer (2019, page 11), including
37 increased resolution and number of stream reaches (2.7 million) for a model covering the
38 contiguous United States (CONUS). A purported strength of WRF-Hydro is simulating
39 hydrologic dynamics, and specifically timing of hydrological response (Salas *et al.*, 2018). The
40 predictive performance of the NWM (ability to match streamflow observations) has been shown
41 to vary widely. Hansen *et al.* (2019) evaluated the performance of the NWM in the Colorado
42 River Basin in terms of drought and low flows; they found better performance in the Upper
43 Colorado River Basin than in the Lower Colorado River Basin, and attributed this discrepancy to
44 the NWM's ability to simulate snowpack. WRF-Hydro has generally poor performance in the
45 Southwest and Northern Plains (Salas *et al.*, 2018). Salas *et al.*, 2018 hypothesized that error in
46 WRF-hydro might come from lakes, reservoirs, floodplain dynamics and soil parameter
47 calibration.

48 NOAA personnel calibrated the NWM (version 2.0) at 1,457 gauged basins within the
49 CONUS domain. As a point of comparison, the United States Geological Survey (USGS) records
50 daily streamflow at 28,529 basins (<https://nwis.waterdata.usgs.gov/nwis>, accessed June 2020).
51 Calibrating the model at each stream gauge within the NWM domain (which include all of
52 CONUS and many U.S. territories) is a large computational expense, and while regionalization
53 strategies can be used to improve real-time forecast accuracy without having to calibrate each
54 individual basin, accuracy typically suffers compared to direct calibration. Due to these reasons
55 and others, making accurate hydrological predictions over large scales is a challenging problem,

1
2
3 56 however there are promising results in the machine learning and data science communities that
4
5 57 may be directly applicable to improving the NWM.
6
7

8 58 Machine learning (ML) is a powerful tool for hydrological modeling, and there has been
9
10 59 a call to merge ML with traditional hydrological modeling (Reichstein *et al.*, 2019; Nearing *et*
11
12 60 *al.*, 2020). One example of an ML approach that has been effective for hydrological prediction is
13
14 61 the “long short-term memory” network (LSTM) (Hochreiter, 1991; Hochreiter and Schmidhuber,
15
16 62 1997). The LSTM is a time series deep learning method that is particularly well suited to model
17
18 63 hydrologic processes because it mimics in certain ways the Markovian input-state-output
19
20 64 structure of a dynamical system (Kratzert *et al.*, 2018). LSTMs have been effective at simulating
21
22 65 predictions of surface runoff at the daily time scale (Kratzert *et al.*, 2019a), including in
23
24 66 ungauged catchments where traditional methods of calibration do not work (Kratzert *et al.*,
25
26 67 2019b), and also at sub-daily (hourly) timescales (Gauch *et al.*, 2020). One potential problem
27
28 68 with ML, however, is that it lacks a physical basis. While there are emerging efforts in hydrology
29
30 69 to merge physical understanding with machine learning (Karpatne *et al.*, 2017a; Daw *et al.*,
31
32 70 2020; Pelissier *et al.*, 2019; Chadalawada *et al.*, 2020; Tartakovsky *et al.*, 2020, Read *et al.*,
33
34 71 2019; Nearing *et al.*, 2020; Hoedt *et al.*, 2021), the field of *theory-guided machine learning*
35
36 72 (Karpatne *et al.*, 2017b) is still relatively immature in hydrology.
37
38
39
40
41
42
43

44 73 The NWM informs forecasts of many hydrologic conditions, including river ice,
45
46 74 snowpack, soil moisture and inundation, which are used for management applications such as
47
48 75 transportation, recreation, agriculture and fisheries (NOAA, 2019). When ML is to be used in the
49
50 76 NWM it should not disrupt the delivery of these hydrologic forecasts, therefore an ML prediction
51
52 77 for streamflow that does not also include predictions of the other hydrologic states and variables
53
54 78 must be run in parallel with the existing process-based hydrologic model. A natural question
55
56
57
58
59
60

1
2
3 79 arises: does the existing NWM formulation benefit the already highly accurate LSTM predictions
4
5 80 of streamflow?
6
7

8 81 Hydrologic post-processing can remove systematic errors in the model prediction, and
9
10 82 has been shown to improve real-time forecast accuracy of both calibrated and uncalibrated
11
12 83 basins, particularly in wet basins (Ye *et al.*, 2014). The general methodology of post-processing
13
14 84 involves taking the output of a process-based model and feeding it into a data-driven model. In
15
16 85 this paper we applied a LSTM-based post-processor for NWM basin-scale streamflow
17
18 86 predictions. This is a straightforward theory-guided machine learning approach. We tested a
19
20 87 LSTM-based post-processor that uses the dynamic NWM model outputs (shown in Table 1 and
21
22 88 described below in the methods section) and compared the results against the NWM itself. We
23
24 89 also tested a post-processor that included both the NWM outputs and atmospheric forcings as
25
26 90 inputs and compared against an LSTM model trained only with atmospheric forcings (no NWM
27
28 91 outputs).
29
30
31
32
33

34 92 We applied the LSTM post-processors to 531 basins across the CONUS. The basins
35
36 93 chosen for this large-scale analysis are mostly headwater catchments without engineered control
37
38 94 structures, such as dams, canals, and levees. This was a deliberate choice made for the purpose of
39
40 95 simulating a close-to-natural rainfall-runoff response. Our goal was to use the post-processor to
41
42 96 learn systematic corrections to simulated basin-scale rainfall-runoff processes that can improve
43
44 97 forecasts of streamflow, rather than the hydraulic engineering implications resulting from
45
46 98 simulated controlled flow, *e.g.* a reservoir release. Kim *et al.* (2020) showed the limitation of the
47
48 99 NWM to predict streamflow in a highly engineered watershed and the need for representing
49
50
51 100 controlled releases. Thus, we are using some of the simplest, and top performing, applications of
52
53
54 101 the NWM for these experiments.
55
56
57
58
59
60

METHODS

Data and Models

CAMELS Catchments. This study used the Catchment Attributes and Meteorological dataset for Large Sample Studies (CAMELS) (CAMELS; Newman *et al.*, 2015; Addor *et al.*, 2017). The US National Center for Atmospheric Research curated these data (NCAR; <https://ral.ucar.edu/solutions/products/camels>, accessed March 2020), and we used the 531 (out of 671) basins that Newman *et al.* (2015) chose for model benchmarking. Newman *et al.* (2015) excluded basins with large discrepancies in different methods for measuring basin area and also basins larger than 2,000 km². CAMELS data include corresponding daily streamflow records from USGS gauges, and meteorological forcing data (precipitation, max/min temperature, vapor pressure and total solar radiation) come from North American Land Data Assimilation System (NLDAS; Xia *et al.*, 2012).

National Water Model. We used the National Water Model version 2.0 reanalysis, which contains output from a 25-year (January 1993 through December 2019) retrospective simulation (<https://docs.opendata.aws/nwm-archive/readme.html>, accessed June 2020). The NWM retrospective ingests rainfall and other meteorological forcings from atmospheric reanalyses (<https://water.noaa.gov/about/nwm>, accessed June 2020). NWM reanalysis output includes channel outputs (point fluxes: CHRT) and land surface (gridded states and fluxes: LDAS and RT) outputs. The specific features that we used from the NWM reanalysis are shown in Table 1. To be compatible with the LSTM model, which uses a one-day timestep and was trained using all basins simultaneously, we took the mean values of these model outputs across UTC calendar days (12AM - 11PM) to produce daily records from the hourly NWM when used as input to the LSTM, but for NWM streamflow diagnostics we used the local calendar day

Revised manuscript submitted to the Journal of The American Water Resources Association (JAWRA) March 2021

125 (based on U.S. time zone) to be compatible with the USGS gauge records. We collected channel
 126 routing point data (CHRT) at each individual NWM stream reach that corresponds to the stream
 127 gauge associated with each CAMELS catchment. We collected the gridded land surface data
 128 (LDAS) from each 1 km² Noah-MP cell (Niu et al., 2011) contained within the boundaries of
 129 each CAMELS catchment, and then calculated the averaged to produce a single representative
 130 (lumped) value for each catchment. We collected Gridded routing data (RT) from each 250 m²
 131 cell, and we included the mean and maximum value within the catchment boundary. We did not
 132 include lake input and output fluxes because these would be inconsistent across basins (some
 133 basins have zero and some basins have multiple lakes). Note that the units of the NWM outputs
 134 are not required for the LSTM post-processor.

135 TABLE 1. National Water Model Output Data

Feature name	Feature	NWM model component	Resolution
ACCET	Accumulated evapotranspiration	LDAS	1km
FIRA	Total net long-wave (LW) radiation to atmosphere	LDAS	1km
FSA	Total absorbed short-wave (SW) radiation	LDAS	1km
FSNO	Snow cover fraction on the ground	LDAS	1km
HFX	Total sensible heat to the atmosphere	LDAS	1km
LH	Latent heat to the atmosphere	LDAS	1km
SNEQV	Snow water equivalent	LDAS	1km
SNOWH	Snow depth	LDAS	1km
SOIL M (4 layers)	Volumetric soil moisture	LDAS	1km
SOIL W (4 layers)	Liquid volumetric soil moisture	LDAS	1km
TRAD	Surface radiative temperature	LDAS	1km
UGDRNOFF	Accumulated underground runoff	LDAS	1km
streamflow	River Flow	CHRT	point
q_lateral	Runoff into channel reach	CHRT	point
velocity	River Velocity	CHRT	point
qSfcLatRunoff	Runoff from terrain routing	CHRT	point
qBucket	Flux from groundwater bucket	CHRT	point
qBtmVertRunoff	Runoff from bottom of soil to groundwater bucket	CHRT	point
Sfheadsbrt (mean and max)	Ponded water depth	RTOUT	250km
Zwattablrt (mean and max)	Water table depth	RTOUT	250km

136

1
2
3 137 **Long short-term memory network.** The LSTM is a recurrent neural network that is able
4
5 138 to maintain a memory of the system state and dynamics through a period of time (in this case 365
6
7 139 days). This recurrent state space is the main advantage for hydrological applications over other
8
9
10 140 types of neural networks. We developed our LSTM network from Kratzert *et al.* (2018, 2019a,b)
11
12 141 using a codebase that is now referred to as NeuralHydrology (<https://neuralhydrology.github.io/>
13
14 142 accessed March 2021). NeuralHydrology was written in the Python programming language and
15
16
17 143 is based primarily on the Pytorch machine learning library.
18
19

20 144 The LSTM in previous studies used two types of inputs: daily meteorological forcings
21
22 145 and static catchment attributes. Again, note that the units of the forcing data are irrelevant when
23
24 146 used as inputs for the LSTM, which does not include a mass or energy balance. We normalized
25
26
27 147 all inputs to the LSTM, including static and dynamic inputs by subtracting the mean and dividing
28
29 148 by the standard deviation of the training data. We used eighteen catchment attributes from the
30
31 149 CAMELS dataset related to climate, vegetation, topography, geology, and soils. These are
32
33
34 150 described in more detail by Addor *et al.* (2017) and listed here in Table 2. Catchment attributes
35
36 151 are static for each basin (do not change in time). With static attributes the LSTM weights and
37
38 152 biases are trained to make predictions that are appropriate for each individual basins, allowing us
39
40
41 153 to train a single model that can be applied on any basin (we tested them on 531 CAMELS
42
43 154 basins). The static attributes position a particular basin within an input space that is suitable for a
44
45 155 particular hydrological response. For instance, the geologic permeability may influence the mass
46
47
48 156 difference between total rainfall and runoff in a particular basin, as it would as a parameter in a
49
50 157 process-based model. For the post-processing runs we added the NWM model output
51
52 158 predictions from version 2.0 of the NWM shown in Table 1.
53
54

55 159 TABLE 2. NLDAS Forcings and Static Catchment Attributes
56
57
58
59
60

Revised manuscript submitted to the Journal of The American Water Resources Association (JAWRA) March 2021

Meteorological Forcing Data (used only in models denoted with an “A”)	
Maximum Air Temp (TMax)	2-meter daily maximum air temperature
Minimum Air Temp (TMin)	2-meter daily minimum air temperature
Precipitation (PRCP)	Average daily precipitation
Radiation (SRAD)	Surface-incident solar radiation
Vapor Pressure (Vp)	Near-surface daily average
Static Catchment Attributes (used in each of the LSTM models)	
Precipitation Mean	Mean daily precipitation
PET Mean	Mean daily potential evapotranspiration
Aridity Index	Ratio of Mean PET to Mean Precipitation
	Estimated by representing annual precipitation and temperature as sin waves
	Positive (negative) values indicate precipitation peaks during the summer (winter).
Precipitation Seasonality	Values of approx. 0 indicate uniform precipitation throughout the year.
Snow Fraction	Fraction of precipitation falling on days with temp [C].
	Frequency of days with $\leq 5x$ mean daily precipitation.
	Average duration of high precipitation events (number of consecutive days with $\leq 5x$ mean daily precipitation).
High Precipitation Frequency	
Low Precipitation Frequency	Frequency of dry days (< 1 mm/day).
	Average duration of dry periods (number of consecutive days with precipitation < 1
Low Precipitation Duration	mm/day).
Elevation	Catchment mean elevation.
Slope	Catchment mean slope.
Area	Catchment area.
Forest Fraction	Fraction of catchment covered by forest.
LAI Max	Maximum monthly mean of leaf area index.
LAI Difference	Difference between the max. and min. mean of the leaf area index.
GVF Max	Maximum monthly mean of green vegetation fraction.
	Difference between the maximum and minimum monthly mean of the green
GVF Difference	vegetation fraction.
Soil Depth (Pelletier)	Depth to bedrock (maximum 50m).
Soil Depth (STATSGO)	Soil depth (maximum 1.5m).
Soil Porosity	Volumetric porosity.
Soil Conductivity	Saturated hydraulic conductivity.
Max Water Content	Maximum water content of the soil.
Sand Fraction	Fraction of sand in the soil.
Silt Fraction	Fraction of silt in the soil.
Clay Fraction	Fraction of clay in the soil.
Carbonate Rocks Fraction	Fraction of the catchment area characterized as “carbonate sedimentary rocks”.
Geological Permeability	Surface permeability (log10).

160

161 We trained the LSTM models to make predictions at all 531 CAMELS catchments used
 162 in the analysis. We split the data temporally into a training period and testing period, and we
 163 present no results from the training period as these results are unrepresentative of the out-of-

1
2
3 164 sample predictions. We trained the LSTMs on water years 2004 through 2014 and tested on
4
5 165 water years 1994 through 2002. We included no spatial splits in the training procedure. The
6
7 166 LSTMs used a 365-day LSTM look-back period, so a full year gap was left between training and
8
9
10 167 testing to prevent bleedover (*i.e.* information exchange) between the two periods. We trained
11
12 168 separate LSTMs with ten unique random seeds for initializing weights and biases, and calculated
13
14 169 benchmarking statistics using the ensemble mean hydrograph. The LSTMs make predictions
15
16 170 representing runoff in units [mm], reflecting an area normalized volume of water that moves
17
18 171 through a stream at each model timestep. USGS gauge records (and the NWM predictions) are in
19
20 172 streamflow units [L^3/T]. We used the geospatial fabric estimate of the catchment area provided
21
22 173 in the CAMELS dataset to convert all streamflow to units [L] for our diagnostic comparison. We
23
24 174 trained the LSTMs with the protocol and features described in Appendix B of Kratzert *et al.*
25
26 175 (2019b): this includes 30 epochs, a hyperbolic tangent activation function, a hidden layer size of
27
28 176 256 cell states, a look-back of 365 days, variable learning rates set at epoch 0 to 0.001, epoch 11
29
30 177 to 0.005 and epoch 21 to 0.0001, dropout rate of 0.4 and an input sequence length: 270.
31
32
33
34
35

36 178 Overfitting of deep learning models can lead to poor performance when the models make
37
38 179 predictions on data that is not part of the training set. The methods described above to ensure that
39
40 180 information in the testing set (water years 1994 through 2002) is not part of the training set helps
41
42 181 build confidence in our modeling results. In addition, the dropout rate is an important hyper-
43
44 182 parameter for preventing overfitting. The dropout probabilistically removed some connections
45
46 183 from the LSTM network during training, in our case with a probability of 0.4. This avoids the
47
48 184 network relying too heavily on specific connections. Model runs during testing did not include
49
50 185 dropout.
51
52
53
54

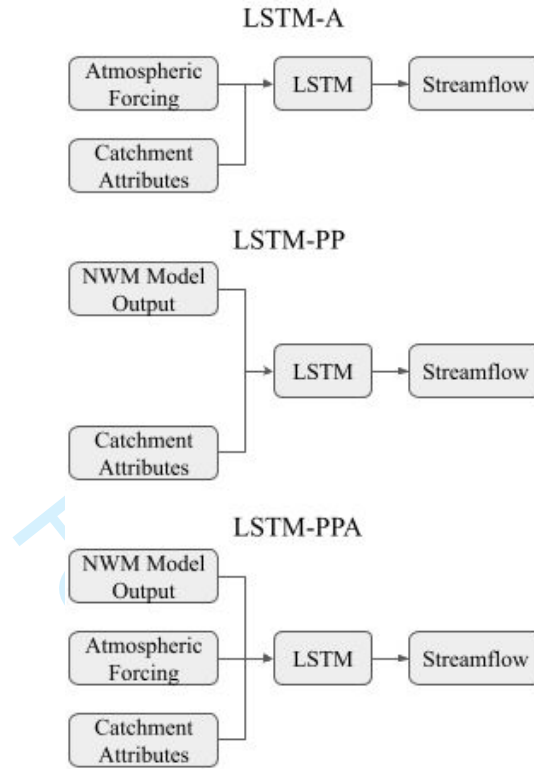
55 186 *Experimental Design*
56
57
58
59
60

187 We tested the results from LSTM post-processing against the NWM and also against a
 188 LSTM trained with atmospheric forcings as dynamic inputs to the model, with no inputs from the
 189 NWM model outputs (referred to as LSTM_A, in which the A stands for atmospheric forcing).
 190 Table 3 will guide the reader through the setup of each model.

191 TABLE 3. Models

Model label	Number of dynamic LSTM inputs	Model description
NWM	N/A	National Water Model mean daily streamflow predictions
LSTM_PP	28	LSTM trained with NWM output for post processing
LSTM_PPA	33	LSTM trained with NWM output and atmospheric forcings for post-processing
LSTM_A	5	LSTM trained with atmospheric forcing conditions.

192
 193 Simple schematics of the LSTMs used in this study are shown in Figure 1. The LSTM
 194 post-processors (LSTM_PP and LSTM_PPA) used NWM outputs as LSTM inputs, and the
 195 process-based NWM predictions influenced the LSTM-based streamflow predictions. This is a
 196 straightforward method of theory-guided (or physics-informed) machine learning, but is
 197 commonly referred to as post-processing (Han, 2021).



198

199 FIGURE 1. Flow chart showing the LSTM_A and the LSTM post-processors with NWM data as inputs (LSTM_PP
 200 and LSTM_PPA). LSTM_PP is the post-processor which used only NWM outputs as input to an LSTM, and
 201 LSTM_PPA used both the NWM outputs and atmospheric forcings.

202 As a quality check, we compared the results from each LSTM ensemble member, and
 203 found a relative standard error of the mean streamflow about 1%, and relative standard error of
 204 the Nash-Sutcliffe Efficiency (NSE) value of about 0.01%. This means that all LSTM solutions
 205 are similar between random initialization seeds. Gauch *et al.* (2019) attributed a 0.01 discrepancy
 206 in NSE values of the LSTM predictions to non-determinism of the loss function minimization. In
 207 our experiments discrepancies in the loss function occur between different random seed
 208 initializations, but running the training procedure twice with the same random seed gives an
 209 identical solution, satisfying the definition of determinism.

1
2
3 210 Model comparisons. We tested/evaluated all models (NWM and all LSTMs) on the same
4
5 211 daily data and the same time period (years 1994-2002). We trained the LSTMs on data from
6
7 212 years 2004-2014 and evaluated them on years 1994-2002. The NWM was calibrated by NOAA
8
9 213 on the time period 2007-2013
10
11
12 214 (https://ral.ucar.edu/sites/default/files/public/9_RafieeiNasab_CalibOverview_CUAHSI_Fall019
13
14 215 [_0.pdf](#), accessed August 2021), though no journal publications thoroughly describe the details of
15
16 216 this calibration. For this study we tested the performance of the NWM reanalysis only on the
17
18 217 time period 1994-2002 (the same time period as the LSTM).
19
20
21

22 218 **Performance metrics.** We calculated several metrics to evaluate predictive performance,
23
24 219 including the NSE and Kling-Gupta Efficiency (KGE) values (Gupta et. al, 2009). We calculated
25
26 220 the variance, bias and Pearson correlation metrics separately as components of the NSE (Gupta
27
28 221 *et al.*, 2009); these tell us about relative variability, mass conservation and linear correlation
29
30 222 between the modeled/observed streamflow values, respectively. Observed streamflow values are
31
32 223 from the USGS streamflow gauges associated with each of the CAMELS basins. We calculated
33
34 224 the metrics in two ways: 1) at each basin and then averaged together, and 2) using all of the
35
36 225 flows from all basins combined.
37
38
39
40

41 226 Our graphical results focus on three performance metrics: (i) NSE measures the overall
42
43 227 predictive performance as a correlation coefficient for the 1:1 linear fit between simulations and
44
45 228 observations, (ii) Peak timing error measures the absolute value of differences (in units days)
46
47 229 between simulated and observed peak flows for a given event, and (iii) total (absolute) bias
48
49 230 measures the overall bias of the simulated hydrograph relative to observations and represents
50
51 231 how well the model matches the total volume of partitioned rainfall that passes through the
52
53 232 stream gauge at each basin.
54
55
56
57
58
59
60

233 We also calculated performance metrics on different flow regimes. Rising limbs and
234 falling limbs were characterized by a one-day derivative, where positive derivatives were
235 categorized as rising limb, and negative derivatives as falling limb. High flows were
236 characterized as all flow above the 80th percentile in a given basin, and low flows as below the
237 20th percentile in a given basin.

238 We tested the performance of the LSTM post-processors in different regions. We split the
239 basins by USGS designated “water resource regions” (<https://water.usgs.gov/GIS/regions.html>,
240 accessed July 2020). To analyze the regions individually we averaged the NSE, bias and timing
241 error of the CAMELS basins within each region.

242 We set an alpha value for statistical significance to $\alpha = 0.05$. To control for multiple
243 comparisons we adjusted the alpha values using family-wise error rate equal to $1-(1-\alpha)^m$, with
244 m being the number of significance tests (86 in total), which brought our effective alpha value
245 down to 0.049. We tested for statistical significance with a Wilcoxon signed-rank test against the
246 null hypothesis that our test models (LSTM post-processors) performance across basins came
247 from the same distribution as our base models (NWM and LSTM_A).

248 **Simulated hydrograph representation of hydrologic signatures.** Hydrologic
249 signatures help us understand how well a model represents important aspects of real-world
250 streamflow, and where improvement should be made to the model's conceptualization (Gupta *et*
251 *al.*, 2008). We analyzed the hydrologic signatures described by Addor *et al.* (2018), and these are
252 listed below in Table 4. We calculated the true signatures with USGS streamflow observations,
253 and calculated model representations with predicted values of daily streamflow. We compared
254 true values and predicted values with a correlation coefficient (r^2) across basins (one value of the

255 observed and predicted hydrologic signatures were calculated per basin), higher values indicate
 256 better representation of hydrologic signature across basins by the model. We used the Steiger
 257 method to test for statistically significant changes between the LSTM_A, NWM and the LSTM
 258 post-processor (Steiger and Browne, 1984).

259 TABLE 4. Hydrologic signatures (adapted from Addor *et al.* 2018)

Signature description	Signature name
Average duration of low-flow events	low_q_dur
Frequency of days with zero flow	zero_q_freq
Average duration of high-flow events	high_q_dur
Streamflow precipitation elasticity	stream_elas
Frequency of high-flow days	high_q_freq
Slope of the flow duration curve	slope_fdc
Frequency of low-flow days	low_q_freq
Baseflow index	baseflow_index
Runoff ratio	runoff_ratio
Mean half-flow date	hfd_mean
5 percent flow quantile	q5
95 percent flow quantile	q95
Mean daily discharge	q_mean

260

261 **Identifying basins best suited for post-processing with multi-linear regression.** The
 262 LSTM post-processors did not improve performance at every basin. It therefore would be
 263 valuable to know if a LSTM post-processor will work in any particular basin before
 264 implementation. We trained a multi-linear regression, using the Scikit-learn library in Python, to
 265 predict the performance changes between the NWM and the LSTM post-processors (LSTM_PP
 266 and LSTM_PPA) at each individual basin. The multi-linear regression analysis included
 267 performance scores of the NWM streamflow predictions, hydrologic signatures and catchment
 268 characteristics as inputs. These regressors are useful to help interpret what basins might benefit
 269 most from an LSTM post-processor. We trained and tested multi-linear regression models using
 270 k-fold cross-validation with 20 splits ($k=20$) over the 531 basins. We report the correlation (r^2)

1
2
3 271 of out-of-sample regression predictions of post-processing changes vs. actual post-processing
4
5 272 changes.

6
7
8 273 **Interpretation of LSTM with integrated gradients.** We aim to explain the relationship
9
10 274 between a model's predictions in terms of its features. This will help us understand feature
11
12 275 importances, identifying data issues, and inform NWM process diagnostics from the post-
13
14 276 processors. We calculated integrated gradients (Sundararajan *et al.*, 2017) to attribute the LSTM
15
16 277 inputs (both atmospheric forcings and NWM outputs) to the total prediction of streamflow.
17
18 278 Integrate gradients are a type of sensitivity analysis that are relatively insensitive to low gradients
19
20 279 (*e.g.*, at the extremes of neural network activation functions). We calculated integrated gradients
21
22 280 separately for each input, at each timestep, for each lookback timestep, in each basin. This means
23
24 281 that for 9 years of test data with a 365-day lookback there were about 1.2 million integrated
25
26 282 gradients per input, per basin. The unit of the integrated gradient is technically normalized
27
28 283 streamflow, but we were mostly interested in the relative values of integrated gradients of each
29
30 284 individual LSTM input.
31
32
33
34
35
36

37 285 **Interpretation of LSTM with correlations between performance and NWM inputs.**
38
39 286 We made a direct connection between LSTM post-processor improvements with the NWM
40
41 287 outputs using correlation. We calculated Pearson R values between the basin average value of
42
43 288 each NWM input feature and the total performance change (NSE, bias and peak timing). We
44
45 289 calculated these correlations for different flow regimes (all flows using the whole hydrograph,
46
47 290 rising/falling limbs using the single day differentials, and high/low flows using the top 80% and
48
49 291 bottom 20%). The strengths of these correlations (positive or negative) indicated which types of
50
51 292 basins (via NWM features) are benefiting most from a LSTM post-processor. Results for rising
52
53
54
55
56
57
58
59
60

limbs and falling limbs of the hydrograph were qualitatively similar to this figure, and were therefore omitted.

Splitting the CAMELS catchments by calibrated / uncalibrated. Of the NWM calibrated basins, 480 overlap with the 531 CAMELS catchments used in this study. In a separate set of experiments, we trained the LSTM_A and the LSTM post-processors (LSTM_PP and LSTM_PPA) on only the 480 calibrated basins. We then used the full set of 531 catchments to test the performance out-of-sample. We analyzed the 480 in-sample basins and 51 out-of-sample basins separately using the NSE, bias and timing error metrics. This allowed us to determine if the LSTM is a suitable post-processing method to use in uncalibrated basins. If the post-processors trained only on calibrated basins can improve streamflow predictions at uncalibrated basins, then they would be considered suitable, particularly if there is no statistical difference between the post-processor's performance improvement over the NWM and/or LSTM_A.

Sensitivity analysis and NWM process diagnostics. We trained a set of LSTM post-processors using different combinations of NWM outputs as input to the LSTM, as described in Table 5. To test the sensitivity to the NWM streamflow prediction itself, we trained an LSTM with only streamflow (LSTM_Q_only), and excluded it from another (LSTM_PP_noQ). We tested the sensitivity to the channel routing (LSTM_chrt) and land surface (LSTM_ldas) components of the NWM by training LSTMs with only these dynamic inputs. We trained these models with the same specifications as the LSTM_A, LSTM_PPA and LSTM_PP.

TABLE 5. Additional models for sensitivity analysis and NWM diagnostics

Model label	Number of dynamic LSTM parameters	Model description
LSTM_PP_noQ	26	LSTM post-processor (LSTM_PP) but without streamflow or velocity.

LSTM_Q_only	1	LSTM trained with NWM streamflow only.
LSTM_chrt	6	LSTM trained with NWM channel routing outputs only.
LSTM_ldas	18	LSTM trained with NWM land surface outputs only.

314

315 Each of these models (Table 5), in addition to the main post-processing models presented

316 in Table 3, have a distinct flow of information that we can use to diagnose NWM model

317 processes. Figure 2 shows the information flow of each of the model subcomponents. We used

318 the performance results of the different post-processing models to assess how much information

319 passes between the model components. Nearing *et al.*, (2018) described the method to quantify

320 the information exchange down a modeling chain (*i.e.*, integrating over the expected effect of the

321 conditional probability), but since we used limited outputs from the NWM reanalysis, rather than

322 the full state space, we examined the NWM only qualitatively for information loss between the

323 major NWM sub-components (land surface runoff, overland router and channel router). The

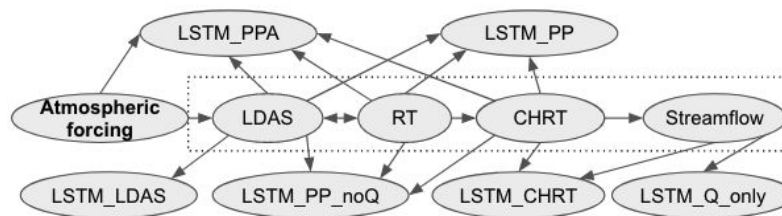
324 LSTM extracts information from its input to make predictions about its target, in our case

325 streamflow, and we assumed higher streamflow prediction accuracy indicated more information

326 is available in the NWM components used as input. If a post-processor made less accurate

327 streamflow predictions than the LSTM_A, then this indicates that the NWM modeling chain lost

328 information from the atmospheric forcings.



329

330 FIGURE 2. Process network diagram showing the information flow of each of these models. Arrows indicate the

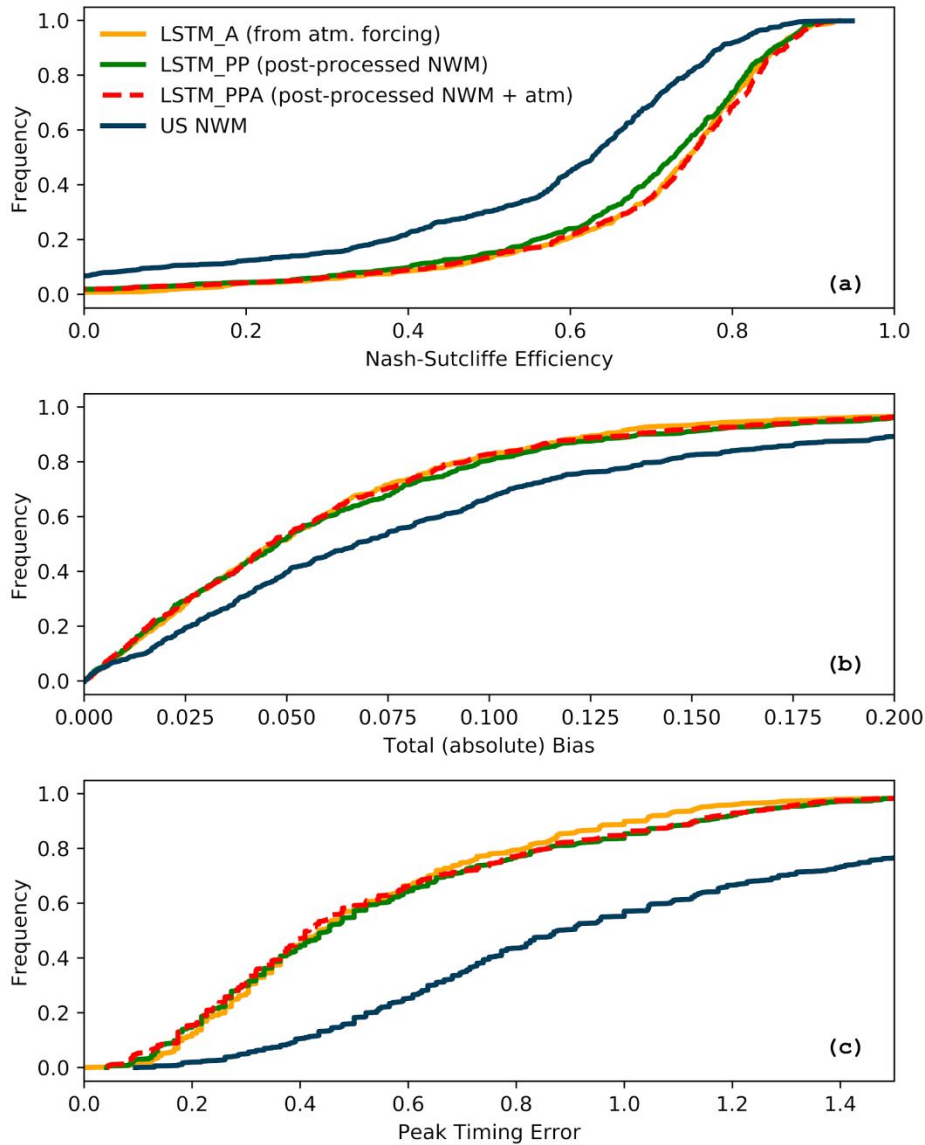
331 information flow from one component of the model to another. The NWM components are outlined with the dashed

332 box. This is also a good guide for understanding the inputs to the different post-processing models.

333 **RESULTS**

334 *Overall model performance*

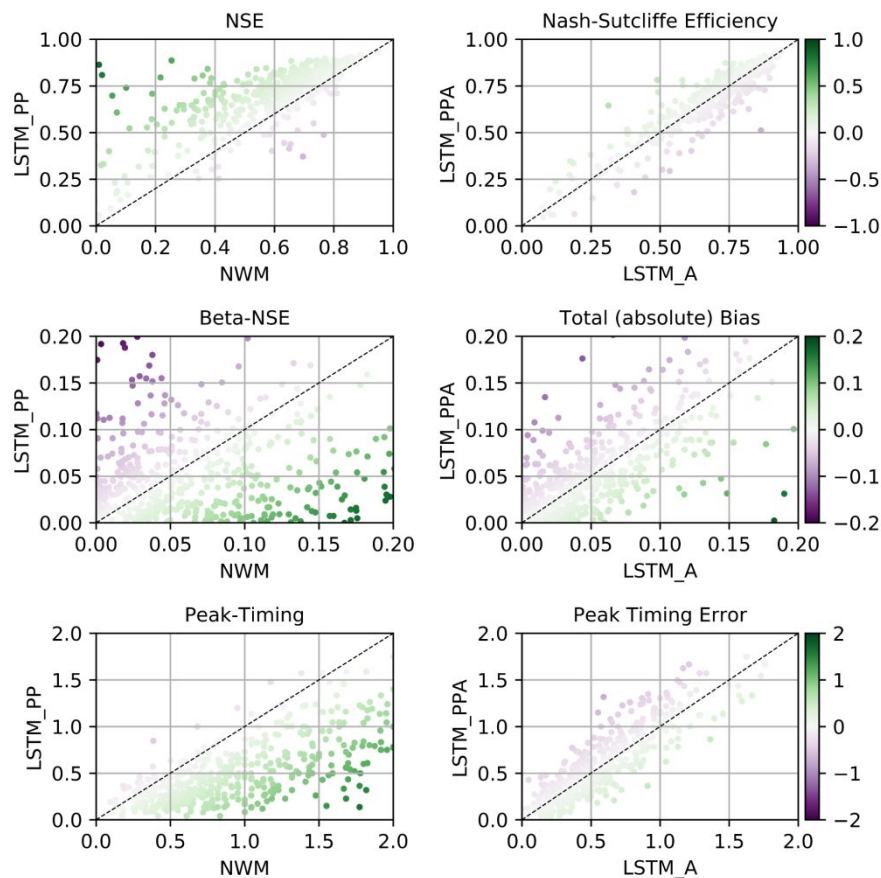
335 Post-processing the NWM with LSTMs significantly improved predictive performance,
 336 both with or without including the atmospheric forcings as inputs into the model. The LSTM_A,
 337 however, is the overall better performing model. Figure 3 shows the cumulative distributions of
 338 three performance metrics (NSE, peak timing error, and total bias).



339

1
2
3 340 FIGURE 3. Results showing the cumulative distributions of model performance calculated as Nash-Sutcliffe
4
5 341 Efficiency (NSE), total bias, and peak timing error over a 10-year test period in 531 CAMELS catchments. The
6
7 342 National Water Model (NWM) reanalysis streamflow was averaged daily, long short-term memory (LSTM)
8
9 343 networks shown used (i) the original atmospheric inputs (LSTM_A), (ii) NWM states and fluxes only (LSTM_PP),
10
11 344 and (iii) both atmospheric forcings and NWM states and fluxes (LSTM_PPA). These figures omit the distribution
12
13 345 tails for clarity.

14
15 346 The LSTM_PP improved the NSE score of the NWM mean daily streamflow at a total of
16
17 347 465 (88%) and reduced accuracy in 66 basins (12%) of the total 531 CAMELS basins, improved
18
19 348 the total bias of the NWM mean daily streamflow at a total of 325 (61%) of basins and improved
20
21 349 the peak timing error at a total of 488 (92%) of basins. The LSTM_PPA post-processor improved
22
23 350 the NSE score of the NWM mean daily streamflow at a total of 488 (92%) and reduced accuracy
24
25 351 in 43 basins (8%) of the total 531 CAMELS basins. The LSTM_PPA post-processor improved
26
27 352 the total bias of the NWM mean daily streamflow at a total of 331 (62%) of basins and improved
28
29 353 the peak timing error at a total of 494 (93%) of basins. The LSTM_A (without NWM model
30
31 354 output) outperformed the NWM at a total of 473 (89%) and reduced accuracy in 58 basins
32
33 355 (11%), improved the total bias of the NWM mean daily streamflow at a total of 339 basins (64%)
34
35 356 and improved the peak timing error at a total of 484 basins (91%). The LSTM_PPA improved
36
37 357 the greatest number of basins in terms of NSE and peak timing error and the LSTM_A was the
38
39 358 best performing model in terms of total bias. Figure 4 shows scatter plots of the post-processor
40
41 359 performance at individual basins against the performance of the NWM and LSTM_A.
42
43
44
45
46
47
48
49
50
51
52
53
54
55
56
57
58
59
60



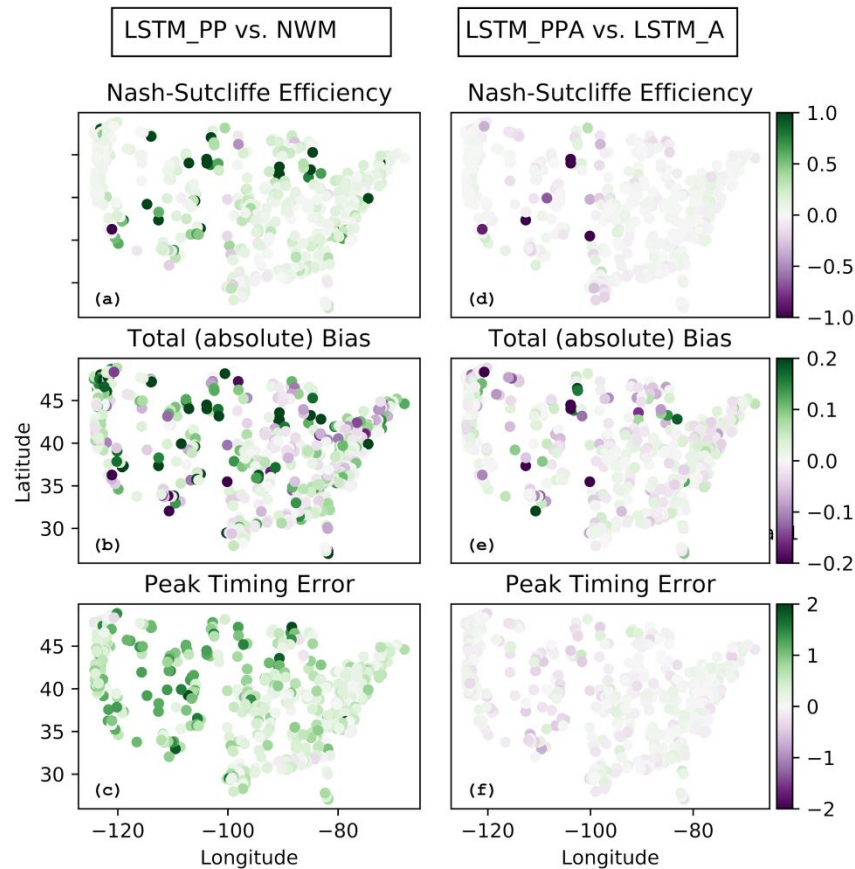
360

361 FIGURE 4. Performance differences of the post-processors against the NWM and LSTM_A in 531

362 CAMELS basins across CONUS. Green indicates basins where post-processing improved performance over the
 363 NWM and LSTM_A (darker indicates larger relative improvement), and purple indicates basins where there was a
 364 decrease in performance (darker indicating worse relative detriment). The first column shows the performance
 365 difference between the LSTM_PP and the NWM. The second column shows the performance difference between
 366 the LSTM_PPA and the LSTM_A.

367 The post-processing models (LSTM_PP and LSTM_PPA) improved relative to the NWM
 368 in similar basins. The improvements of the two post-processing methods are correlated across all
 369 basins ($r^2 = 0.995$). Performance comparisons between the LSTM models and the NWM for
 370 each basin are plotted spatially in Figure 5. Notice that some of the highest NSE improvements
 371 between the LSTM_PP and the NWM are the worst NSE detriments between the LSTM_PPA

372 and the LSTM_A, particularly in the northern plains. This indicates that although the post-processor greatly improves the NWM, the information from the NWM at bad basins hinders the
 373 processor greatly improves the NWM, the information from the NWM at bad basins hinders the
 374 performance of the LSTM, or in other words, the NWM passes bad information to the LSTM.



375
 376 FIGURE 5. Per-basin performance change between the post-processors and NWM and LSTM_A in 531
 377 CAMELS basins across CONUS. Green indicates basins where post-processing improved performance over the
 378 NWM and LSTM_A (darker indicates larger relative improvement), and purple indicates basins where there was a
 379 decrease in performance (darker indicating worse relative detriment). The first column (a-c) shows the performance
 380 change between the LSTM_PP and the NWM. The second column (d-f) shows the performance change between the
 381 LSTM_PPA and the LSTM_A.

382

383 *Performance by flow regime*

384 The LSTM post-processors improved predictive performance of the NWM according to
 385 the NSE and KGE metrics, as well as their components (variance and correlation). A full set of
 386 performance metrics broken down by flow regime are shown in Table 6. The left side of the table
 387 shows the average of metrics calculated individually at each basin, and the right side of the table
 388 shows the metrics as calculated combining the flows from all basins. The NSE includes both
 389 mean and median averages, but the rest of the metrics are only averaged by median.

390 TABLE 6. Predictive performance for NWM, LSTM_A and the LSTM Post-processors during various flow
 391 regimes. The Nash-Sutcliffe Efficiency (NSE) and Kling-Gupta Efficiency (KGE) are overall performance metrics
 392 of prediction quality. Variance, bias and correlation (R) are the components of the NSE. We calculated these in two
 393 ways: 1) at each basin and averaged across all basins, and 2) once using the observed and predicted streamflow
 394 values from all basins combined. Note that calculations done once across all basins do not include a test of
 395 significance.

Flow categories		Calculated per-basin						All basins			
All flows	NSE (mean)	NSE (median)	KGE	variance	bias	R	NSE	variance	bias	R	
NWM	0.46	0.62	0.64	0.82	-0.01	0.82	0.75	0.85	-0.02	0.87	
LSTM_PP	0.65*	0.73*	0.74*	0.86	0.02	0.87*	0.81	0.92	0.02	0.90	
LSTM_A	0.69	0.74	0.74	0.83	0.02	0.88	0.82	0.89	0.01	0.90	
LSTM_PPA	0.67	0.75	0.76	0.87	0.02	0.88	0.82	0.93	0.02	0.91	
Rising limbs	NSE (mean)	NSE (median)	KGE	variance	bias	R	NSE	variance	bias	R	
NWM	0.47	0.60	0.60	0.77	-0.07	0.81	0.73	0.82	-0.05	0.85	
LSTM_PP	0.64*	0.70*	0.72*	0.83*	0.00*	0.86*	0.78	0.88	0.00	0.88	
LSTM_A	0.66	0.71	0.72	0.80	-0.01	0.86	0.78	0.85	-0.01	0.88	
LSTM_PPA	0.65	0.72	0.74	0.85	0.00	0.87	0.79	0.89	0.00	0.89	
Falling limbs	NSE (mean)	NSE (median)	KGE	variance	bias	R	NSE	variance	bias	R	
NWM	0.29	0.62	0.64	0.94	0.03	0.83	0.78	0.90	0.00	0.88	
LSTM_PP	0.62*	0.75*	0.76*	0.95*	0.07	0.90*	0.87	0.99	0.04	0.93	
LSTM_A	0.69	0.78	0.77	0.92	0.05	0.90	0.87	0.96	0.03	0.93	
LSTM_PPA	0.65	0.77	0.77	0.94	0.05	0.90	0.87	0.98	0.03	0.93	
Above 80th percentile	NSE (mean)	NSE (median)	KGE	variance	bias	R	NSE	variance	bias	R	

	NWM	0.17	0.41	0.54	0.80	-0.13	0.73	0.69	0.83	-0.10	0.84
	LSTM_PP	0.47*	0.57*	0.64*	0.82	-0.08*	0.80*	0.76	0.89	-0.04	0.90
	LSTM_A	0.53	0.58	0.67	0.81	-0.08	0.81	0.78	0.86	-0.06	0.88
	LSTM_PPA	0.50	0.60	0.69	0.84	-0.07	0.81	0.79	0.90	-0.04	0.89
	Below 20th percentile										
		NSE (mean)	NSE (median)	KGE	variance	bias	R	NSE	variance	bias	R
	NWM	-18384.37	-17.47	-1.96	3.79	1.89 [^]	0.36	0.37	1.31	0.22	0.81
	LSTM_PP	-6941.62*	-15.66*	-1.28*	2.84*	3.21	0.43*	0.53	1.30	0.33	0.90
	LSTM_A	-4749.68	-16.35	-1.31	2.85	3.27	0.43	0.56	1.26	0.33	0.89
	LSTM_PPA	-5147.62	-14.66	-1.24	2.85	2.87	0.43	0.58	1.28	0.30	0.90

Note: * indicates post-processing significantly helps the NWM

Note: ^ indicates post-processing significantly hurts the NWM

396

397 In general Table 6 shows that the LSTM post-processors improved over the NWM in
 398 nearly all flow regimes according to most metrics. The LSTM_PPA also improved upon the
 399 LSTM_A in more than half the basins, and by most metrics, though not significantly. The
 400 prediction of rising limb and high flow regimes were improved upon by the LSTM post-
 401 processors according to every metric.

402 Bias was the only metric that was reduced due to post-processing, and the difference was
 403 highest in low flow regimes. All models poorly predicted flows below the 20th percentile. This is
 404 likely due to the fact that all models tend to have difficulty predicting zero streamflow, and the
 405 101 basins with periods of zero streamflow affected the average performance metrics. This will
 406 be discussed further in terms of hydrologic signatures.

407 The right side of the table has better performance values than the average of metrics
 408 calculated individually at each basin. This is a result of some of the better performing basins
 409 compensating for poorer performing basins, or from a different perspective, some basins have
 410 relatively poor performance which weighs down the average.

1
2
3 411 *Performance by region*
4
5

6 412 Results from a regional analysis of performance are shown below in Figure 6. The
7
8 413 LSTM post-processors significantly improved the NSE over the NWM in fifteen of the eighteen
9
10 414 regions, the peak timing error in sixteen regions (all regions with enough basins for a statistical
11
12 415 evaluation) and significantly improved bias in only one region. Note that region 9 was
13
14 416 represented by only two CAMELS basins, which is not sufficient for statistical evaluation. The
15
16 417 bias was better represented by the NWM than the post-processor in five of the eighteen regions,
17
18 418 including the entire East Coast (regions 1, 2 and 3), the Pacific Northwest (17) and the Lower-
19
20 419 Colorado River (15).
21
22
23
24

25 420 The regional performance of the LSTM post-processors and the regional performance of
26
27 421 the LSTM_A were correlated with the regional performance of the NWM in terms of NSE
28
29 422 ($r^2=0.78$ for post-processors and 0.63 for LSTM_A) and peak timing error ($r^2=0.96$ for post-
30
31 423 processors and 0.92 for LSTM_A), but not in terms of bias ($r^2=0.24$, calculated on bias although
32
33 424 absolute bias is plotted for clarity). The post-processors and the LSTM_A are correlated in terms
34
35 425 of their bias ($r^2=0.91$). A better model has a higher NSE, bias closer to zero, and a lower timing
36
37 426 error.
38
39
40
41
42
43
44
45
46
47
48
49
50
51
52
53
54
55
56
57
58
59
60

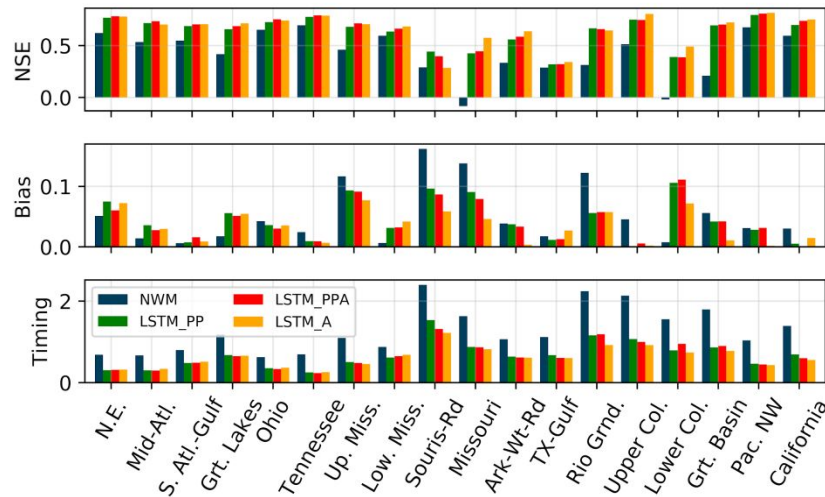
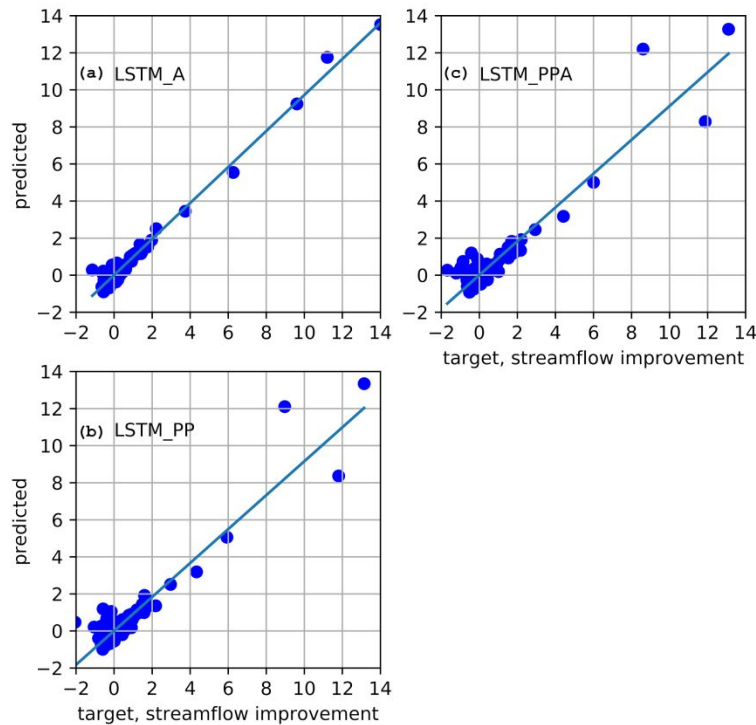


FIGURE 6. Regionally averaged performance metrics for NWM, LSTM_A, and the LSTM post-processors (LSTM_PP and LSTM_PPA) in different USGS water resources regions.

Regression to predict post-processing performance improvement

The performance of the LSTM_A was more predictable than the post-processors. We performed a multi-linear regression on the target of performance improvement over the NWM, with inputs being the catchment attributes and hydrologic signatures, as well as the NWM performance itself. Figure 7 shows the results predicting the LSTM improvement over the NWM at each basin with an r^2 value of 0.97, 0.88 and 0.89 for the LSTM_A, LSTM_PPA and LSTM_PP, respectively. The high r^2 value is due in part to the outlier basins with abnormally large performance improvements from the LSTM models (LSTM_A, LSTM_PPA and LSTM_PP). This means that the magnitude of the LSTM_A and post-processors improvement is directly related to the performance of the NWM.



440

441 FIGURE 7. Predicting LSTM_A, LSTM_PP and LSTM_PPA performance over the NWM at each basin using a

442 linear regression with NWM performance and hydrologic signatures as inputs. Scatter plots with all of the 531

443 basins.

444

445 The aim of these results is to understand whether it is possible to predict where post-

446 processing might be beneficial (remember that post-processing helped in most basins). Although

447 we found relatively high predictability in the improvement expected from post-processing, a

448 problem is that this requires knowing ahead of time the NWM performance. This prevents us

449 from predicting post-processing improvement in *ungauged* basins, since calculating the NWM

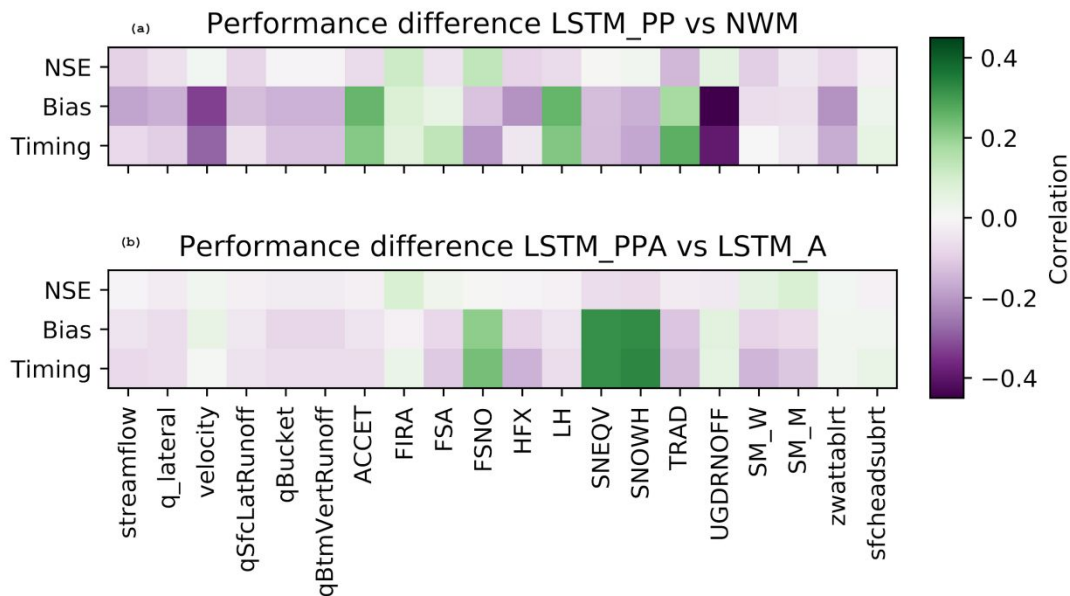
450 performance requires streamflow observations. The correlation analysis below may help inform

1
2
3 451 future efforts to learn general patterns of post-processor improvement over both the NWM and
4
5 452 the LSTM_A.
6
7

8 453
9
10

11 454 *Correlations between NWM inputs and improvements*
12
13

14 455 Figure 8 shows correlations (over 531 basins) between the time-averaged NWM inputs
15
16 456 and changes in performance metric scores of the post-processor relative to the NWM and
17
18 457 LSTM_A. The LSTM_PP was compared against the NWM and the LSTM_PPA was compared
19
20 458 against the LSTM_A, although qualitatively both post-processor models were similar. The rows
21
22 459 of this figure show that correlation was weaker for differences in NSE score than total bias and
23
24 460 peak timing error. Performance differences between the NWM and the post-processor were most
25
26 461 strongly (anti)correlated with stream velocity from the channel router and accumulated
27
28 462 underground runoff from the land surface model component: basins with lower stream velocity
29
30 463 (velocity) and less underground runoff (UGDRNOFF) saw greater performance improvement
31
32 464 from (daily) post-processing. This means that in basins with high underground runoff and/or high
33
34 465 stream velocity the post-processor improvements were smaller. In contrast, basins with higher
35
36 466 total radiation (TRAD) and higher latent heat flux (LH) saw greater improvement due to post-
37
38 467 processing. This means that in basins with more radiation and heat flux the post-processor
39
40 468 improvements were larger. A direct interpretation of this could be that a flat meandering stream
41
42 469 in the Southwest will benefit from post-processing, which is consistent with the findings of Salas
43
44 470 *et al.* (2018) that WRF-Hydro's performance is generally poor in the Southwest. Performance
45
46 471 differences between the LSTM_A and the post-processor were most strongly correlated with
47
48 472 snow water equivalent and snow depth. This is consistent with the findings of Hansen *et al.*
49
50 473 (2019) that the NWM represents snowpack hydrology well.
51
52
53
54
55
56
57
58
59
60

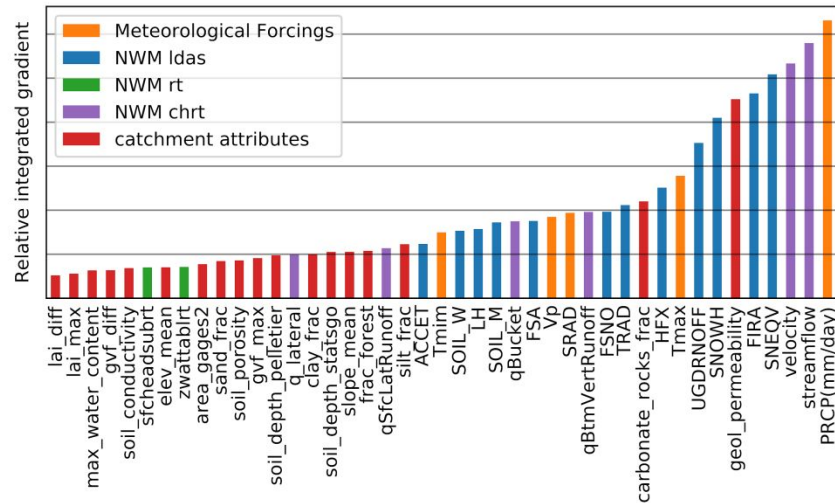


474
475 FIGURE 8. Correlations between the time-averaged NWM related inputs vs. performance metric differences
476 between the LSTM post-processors (LSTM_PP and LSTM_PPA) and NWM and LSTM_A.

477 *Integrated gradients*

478 Figure 9 shows the relative strength of the total attribution of the dynamic inputs to the
479 LSTM_PPA averaged across the entire validation period and across basins. The ordered
480 magnitudes of the integrated gradients can be interpreted as corresponding to the order of
481 importance of inputs. The most important dynamic features for the LSTM_PPA were: (i)
482 precipitation from NLDAS, and (ii) routed streamflow from the NWM point data. Precipitation
483 inputs were weighted higher than the NWM streamflow output itself, which means that even
484 when NWM streamflow data were available, the LSTM_PPA generally learned to get
485 information directly from forcings rather than from the NWM streamflow output. This indicates
486 that the LSTM_PPA generated a new rainfall-runoff relationship rather than relying on the

487 NWM, which is consistent with the overall results (Figure 2) that showed similar performance
 488 between the LSTM_A and LSTM_PPA.



489
 490 FIGURE 9. Attributions to the LSTM_PPA predictions. The vertical axis shows the relative magnitude of attribution
 491 (importance) for each input, with precipitation (PRCP) as the top contributor and NWM-predicted runoff into
 492 channel reach ($q_{lateral}$) contributing the least.

493 Figure 10 shows the relative strength of the total attribution of the dynamic inputs to the
 494 LSTM_PP. Without the atmospheric forcings included in the post-processor inputs the NWM
 495 streamflow output was by far the highest contributing dynamic input feature to the LSTM_PP.
 496 The static permeability of the catchment was the next highest.

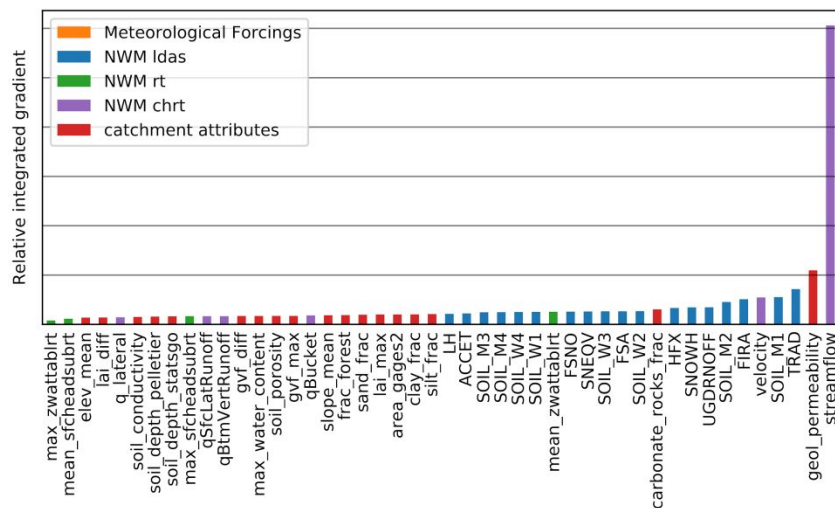
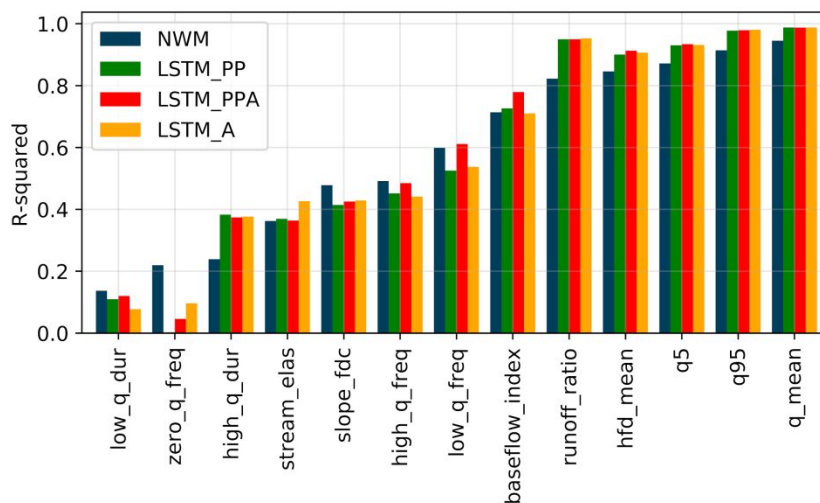


FIGURE 10. Attributions for the LSTM_PP model. Color coded by LSTM input source. The streamflow is overwhelmingly the highest contributor to the post-processed streamflow prediction.

Representations of hydrologic signatures

Results of the analysis of hydrologic signature representation are shown in Figure 11, which also shows that the hydrologic signatures best represented by the NWM were similarly those best represented by the LSTM_PPA. The same was true for the most poorly represented hydrologic signatures in both models.



505

1
2
3 506 FIGURE 11. Correlation between simulated and observed per-basin hydrologic signatures from the NWM (blue),
4
5 507 LSTM_A (orange), LSTM_PPA (green), and LSTM_PP (red). Larger values indicates better performance..
6

7
8 508 The LSTM post-processors hurt the representation of the frequency of days with zero
9
10 509 flow. There were 101 basins with any periods of zero flow. None of these models do well
11
12 510 simulating zero flow, but the NWM is better at handling this situation, predicting zero flow
13
14 511 periods in 56 of the 101 basins. The LSTM_A, LSTM_PPA and LSTM_PP only predicted
15
16 512 periods of zero flows at 35, 29 and 25 basins, respectively. This is an important characteristic in
17
18 513 basins in the Southwest, where the NWM could use the benefit of a LSTM post-processor, so
19
20 514 this would be a good place to focus future research of theory-guided ML for hydrology.
21
22
23

24 515 The LSTM post-processor made a significant improvement over the NWM for several
25
26 516 signatures. The improvement to runoff ratio, which is the fraction of precipitation that makes it
27
28 517 through the stream gauge at the surface, could be a compensation for the uncalibrated soil
29
30 518 parameters in the NWM mentioned by Salas *et al.* (2018). The LSTM post-processor improved
31
32 519 both high and low flow predictions (5% and 95% flow quantiles), which are important for natural
33
34 520 resources management. Mean daily discharge was the best represented hydrologic signature by
35
36 521 all models.
37
38
39
40

41 522 The LSTM_PPA post-processor made significant improvements over the LSTM for
42
43 523 baseflow index. This is the only signature that an LSTM post-processor improved over both the
44
45 524 NWM and the LSTM_A. This signature estimates the contribution of baseflow to the total
46
47 525 discharge, which is computed by hydrograph separation. Klemeš (1986) (summarizing Lindsly's
48
49 526 Applied Hydrology) cautioned strongly against using hydrograph separation, because there is no
50
51 527 real basis for distinguishing the source of flow in a stream.
52
53
54
55

56 528 *Results comparing gauged basins vs. ungauged basins*
57
58
59
60

Results in Table 9 summarize an analysis designed to replicate prediction in ungauged basins. The table has metrics from predictions by the NWM, LSTM_A and the LSTM post-processors (LSTM_PP and LSTM_PPA) calculated only at basins that were either calibrated or uncalibrated, but not both. There was no statistical difference between the calibrated and uncalibrated samples. This indicates that the LSTM post-processor works in uncalibrated basins. When post-processors were trained only in calibrated basins (denoted with a “C” in Table 9), however, the performance in uncalibrated basins significantly deteriorated. But this is true for the LSTM_A as well, so it is not a result of the calibration (as calibration would not influence the LSTM_A), but a result of prediction at ungauged type basins. However, the median performance of the post-processor predictions at ungauged type basins when trained at only calibrated basins was still significantly better than the NWM in the uncalibrated basins.

TABLE 9. Performance of the LSTM and the LSTM post processor split between basins where the NWM was calibrated vs. uncalibrated. The “C” in the model name denotes that the model training set only included calibrated basins.

Nash-Sutcliffe Efficiency									
	Calibrated basins				Uncalibrated basins				
	mean	median	max	min	mean	median	max	min	
NWM	0.49	0.64	0.95	-10.81	0.18	0.48	0.79	-7.10	
LSTM_PP	0.65	0.73	0.93	-3.32	0.69	0.71	0.89	0.38	
LSTM_A	0.68	0.74	0.93	-0.64	0.73	0.75	0.89	0.43	
LSTM_PPA	0.66	0.75	0.93	-3.61	0.71	0.73	0.89	0.42	
LSTM_PP(C)	0.65	0.73	0.93	-1.86	0.21	0.57	0.75	-8.12	
LSTM_A(C)	0.67	0.74	0.93	-1.13	0.51	0.67	0.84	-2.54	
LSTM_PPA(C)	0.67	0.75	0.94	-2.71	0.13	0.58	0.84	-14.07	

Total bias									
	Calibrated basins				Uncalibrated basins				

	mean	median	max	min	mean	median	max	min	
NWM	0.01	-0.01	2.57	-0.63	0.00	-0.06	1.84	-0.58	
LSTM_PP	0.04	0.02	1.05	-0.24	0.02	0.01	0.27	-0.12	
LSTM_A	0.02	0.02	0.56	-0.22	0.02	0.01	0.20	-0.11	
LSTM_PPA	0.03	0.02	0.98	-0.21	0.01	0.00	0.22	-0.11	
LSTM_PP(C)	0.01	-0.01	0.92	-0.25	0.06	-0.04	2.15	-0.51	
LSTM_A(C)	0.02	0.02	0.62	-0.21	0.09	0.04	0.99	-0.20	
LSTM-PPA(C)	0.01	0.00	0.95	-0.22	0.06	-0.05	2.89	-0.41	
Peak timing error									
	Calibrated basins				Uncalibrated basins				
	mean	median	max	min	mean	median	max	min	
NWM	1.06	0.91	3.00	0.10	1.04	0.77	2.70	0.25	
LSTM_PP	0.55	0.45	1.95	0.04	0.52	0.35	1.59	0.04	
LSTM_A	0.53	0.43	1.76	0.00	0.51	0.41	1.50	0.04	
LSTM_PPA	0.54	0.42	1.75	0.04	0.51	0.36	1.45	0.05	
LSTM_PP(C)	0.55	0.45	2.10	0.00	0.59	0.41	1.76	0.09	
LSTM_A(C)	0.52	0.43	1.77	0.00	0.57	0.50	1.50	0.08	
LSTM_PPA(C)	0.54	0.41	1.83	0.04	0.57	0.41	1.65	0.13	

543

544 The NWM, LSTM_A and the LSTM_PPA had higher NSE scores in calibrated basins
545 than the uncalibrated basins. Note that these results are from the LSTMs (with and without
546 NWM model outputs) trained on only basins where the NWM was calibrated. In the case of the
547 LSTM post-processors the mean NSE scores in uncalibrated basins were very low for NSE. This
548 is a result of two outlier basins (1466500, MCDONALDS BRANCH, Lat:39.9, Lon:-74.5, Area:
549 5.7km; and 01484100 BEAVERDAM BRANCH, Lat:38.9, Lon:-75.5, Area: 7.8km). Both of
550 those outlier basins are much smaller, and have lower flows, than the average of the training set.

1
2
3 551 Without these basins the mean NSE scores were 0.32, 0.51, 0.56 and 0.56 for the NWM,
4
5 552 LSTM_PP, LSTM_A and LSTM_PPA, respectively. Table 9 also shows that the median value of
6
7 553 the LSTM_PPA was higher than the NWM, as was the maximum NSE value, but the minimum
8
9 554 value was exceptionally low.

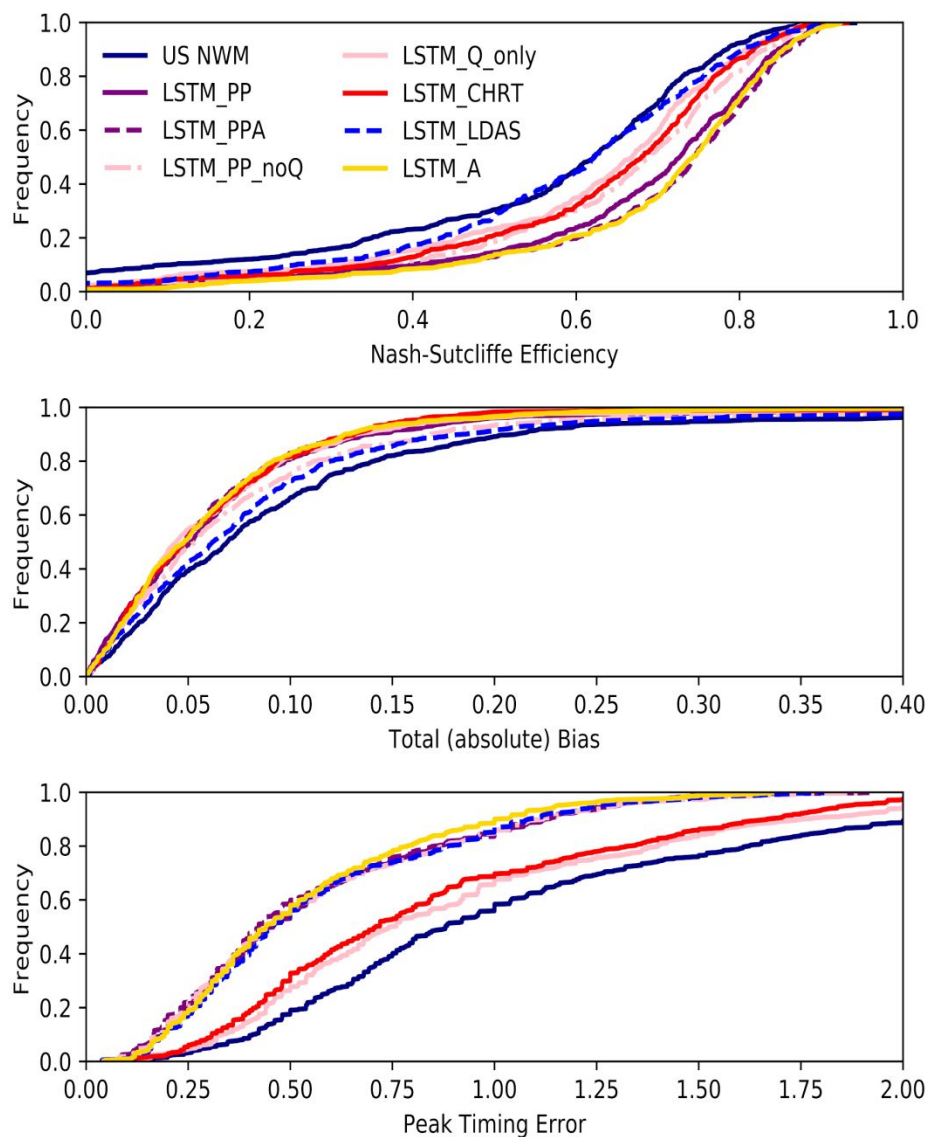
10
11
12
13 555 The total bias in calibrated basins was generally better (lower) than the uncalibrated
14
15 556 basins. The timing error of the NWM was actually better in the uncalibrated basins, but the
16
17 557 LSTM_A and LSTM post-processors had better performance in the calibrated basins. The NSE
18
19 558 values for the NWM, LSTM_A and the LSTM post-processors (LSTM_PP and LSTM_PPA)
20
21 559 were significantly different in the calibrated basins vs. the uncalibrated basins, as were the
22
23 560 differences between the LSTM_A and LSTM post-processors (LSTM_PP and LSTM_PPA)
24
25 561 compared to the NWM. The bias values were significantly different between the two samples
26
27 562 (calibrated vs. uncalibrated), but the differences between LSTM_A and LSTM post-processors
28
29 563 vs. the NWM were not statistically different. This means that the LSTM models were successful
30
31 564 at predicting streamflow at basins outside of the calibration set.

32
33
34
35
36
37 565 *LSTM post-processor sensitivity to inputs and application for process representation*
38
39 566 *diagnostics.*

40
41
42 567 Figure 12 shows results from the LSTM models with inputs from different parts of the
43
44 568 NWM (land surface model only, channel router only, predicted streamflow only, and all states
45
46 569 and fluxes., . The best performing LSTM models (LSTM_A and LSTM_PPA) were the ones
47
48 570 trained with inputs that included the five atmospheric forcing variables with (LSTM_PPA) and
49
50 571 without (LSTM_A) the NWM output (these are the same models discussed in previous sections
51
52 572 above). This implies that LSTM in general was able to extract more information from the
53
54 573 atmospheric forcings than the NWM. Each of the LSTM post-processors made better average
55
56
57
58
59
60

1
2
3 574 daily streamflow predictions than the NWM itself, indicating that information from the
4
5 575 atmospheric forcings is lost in the NWM model structure before the streamflow prediction is
6
7 576 made. For example, the LSTM that took as inputs only the LDAS model output from the NWM
8
9
10 577 made better predictions than the NWM itself, indicating that there is more information in the
11
12 578 LDAS states and fluxes than the NWM is able to translate into streamflow predictions. The same
13
14
15 579 was true for the states and fluxes of the CHRT component of the NWM, meaning that
16
17 580 information is also lost in the CHRT component of the NWM model structure.
18
19
20 581

For Peer Review



582

583 FIGURE 12. Performance of the LSTM post-processor trained with different sets of NWM output. Each of
 584 these post-processors outperform the NWM. LSTM_A is the LSTM trained with atmospheric forcings as dynamic
 585 inputs. LSTM_PP is the NWM post-processor trained with the outputs of the NWM as dynamic inputs. LSTM_PPA
 586 used both the NWM outputs and atmospheric forcings as inputs. LSTM_PP_noQ used all the NWM outputs except
 587 for streamflow and velocity from the channel router. LSTM_Q_only used only streamflow from the NWM output.
 588 LSTM_chrt used only the NWM channel router outputs. LSTM_ldas used only the land surface fluxes as inputs.

589

DISCUSSION

1
2
3 590 *Comparison between the LSTM_A and the post-processors (LSTM_PP and LSTM_PPA)*
4
5

6 591 The LSTM_A, trained only on atmospheric forcings as dynamic inputs, was better at
7
8 592 extrapolating hydrologic conditions outside the training set than the LSTM post-processors
9
10 593 (LSTM_PP and LSTM_PPA), and thus LSTM_A is the better performing model. This is shown
11
12 594 in the analysis of prediction in ungauged basins, specifically Table 9. The post-processors both
13
14 595 failed to make reasonable predictions at two basins that were much smaller than any basins
15
16 596 included in the training set. The LSTM_A was able to make good predictions in these basins.
17
18 597 Including the NWM output as dynamic inputs to the LSTM constrained the model and prevented
19
20 598 it from learning general hydrologic relationships that can be extracted to basins with
21
22 599 characteristics that might be unrecognizable.
23
24
25
26
27

28 600 *Potential for improving the performance of both the National Water Model and machine*
29
30 601 *learning*
31
32

33 602 Results presented here show that the LSTM post-processors are unreliable for improving
34
35 603 predictions of the NWM. The LSTM post-processors did provide significant benefit to the NWM
36
37 604 streamflow predictions at almost all (88% and 92% for LSTM_PP and LSTM_PPA,
38
39 605 respectively) of the 531 basins analyzed here, but was severely detrimental to two basins in our
40
41 606 tests of ungauged basins. In these basins where this was not the case, it may be possible to use
42
43 607 fine tuning a version of the post-processor that is specific to each gauge location (as would be
44
45 608 done in traditional model calibration), however the LSTM_A did not have this problem and is
46
47 609 more reliable. We trained the LSTMs on headwater basins, so further work would be needed to
48
49 610 include reservoirs, urban areas and other management practices. It is worth noting that these
50
51 611 LSTM models can be trained on a laptop computer in a few hours, a relatively minor
52
53
54 612 computational cost, and the computational cost of forward prediction is negligible. By
55
56
57
58
59
60

1
2
3 613 comparison the computational cost of calibrating the NWM is much higher - typically requiring
4
5 614 HPC or cloud systems.
6
7

8 615 The NWM performance and the performance improvement from the LSTM post-
9
10 616 processors (LSTM_PP and LSTM_PPA) were negatively correlated: basins with low
11
12 617 performance by the NWM have the highest performance change from the LSTM post-
13
14 618 processors. This means that post-processing can be expected to correct situations where the
15
16 619 NWM gives bad predictions. Conversely, the performance of the NWM and the LSTM_A (the
17
18 620 LSTM trained without NWM model outputs) were minimally correlated (r-squared = 0.42, 0.30
19
20 621 and 0.67 for NSE, bias and timing, respectively). Considering also that the overall performance
21
22 622 of the LSTM_A changed only minimally from the addition of the NWM inputs (as shown in
23
24 623 Figures 3-5 and Table 6) and that the LSTM_PPA still preferred to extract more information
25
26 624 from precipitation forcings (shown in Figure 9), we might conclude that the LSTM post-
27
28 625 processors learned new patterns of the rainfall-runoff response, which are not fully represented
29
30 626 by the NWM. But this relationship is also learned by LSTM_A, without the influence of the
31
32 627 NWM. The overall improvement in the representation of hydrologic signatures indicates the
33
34 628 post-processor may be a better representation of physical flow patterns than either the NWM or
35
36 629 the LSTM_A, though not significantly. The interpretation of the integrated gradient (Figures 9
37
38 630 and 10) and the correlations between improvement and NWM features (Figure 8) indicate that
39
40 631 this improvement of flow patterns comes from information in the NWM representation of
41
42 632 streamflow and snow states.
43
44
45
46
47
48
49

50 633 *Application to real-time forecasting*

51
52
53 634 The NWM is not simply a rainfall-runoff simulator; it simulates flow through 2.7 million
54
55 635 river reaches around CONUS, dam operations, land surface processes, hydraulics, and other
56
57
58
59
60

1
2
3 636 complications of large domain hydrology. The nature of the CAMELS catchments selected in
4
5 637 these experiments are such that they have few engineered control structures, and are under
6
7 638 20,000 km². The results presented in this paper show that the LSTMss improved streamflow
8
9 639 predictions in the catchments studied here, which all had limited human disturbance (*e.g.*, dams,
10
11 640 reservoirs, *etc.*). Kratzert *et al.* (2019a) showed that LSTM_A predictions extend into ungauged
12
13 641 basins, and this is consistent with our results. Our results (section “*Results comparing calibrated*
14
15 642 *basins vs. uncalibrated basins*”) show that the LSTM_A is a much better choice than the post-
16
17 643 processors in ungauged basins, which is the majority of the NWM domain. The immediate
18
19 644 potential for improving real-time forecasting could be deploying an LSTM_A for streamflow
20
21 645 prediction in undisturbed catchments, and undisturbed sub-catchments upstream of unnatural
22
23 646 hydrologic conditions such as dams, agriculture lands and urban centers. This would allow for
24
25 647 retaining conceptual representations of lakes and reservoirs that already exist in the NWM.

26
27
28
29
30
31 648 *Diagnosing process-based models, physical processes and data concerns*

32
33
34 649 The sensitivity analysis reported in Figure 12 showed that some components of the NWM
35
36 650 caused poor predictions. Specifically information was lost in channel router (CHRT) component
37
38 651 of the model. This diagnostic method could be used to compare different schemes for future
39
40 652 versions of the NWM. For instance, changing the routing function might conserve timing
41
42 653 information from the land surface fluxes, or modifying the evapotranspiration options in Noah-
43
44 654 MP may conserve mass bias information from the NWM forcing engine. Such improvements
45
46 655 could be quantified with this post-processing method.

47
48
49
50
51 656 Each of the post-processing models tested for sensitivity (Figure 12) fall, roughly and
52
53 657 inclusively, between the NWM and the LSTM_A. Based on the relative positions between those
54
55 658 bounding curves, we can identify sources of information loss through the NWM modeling chain:

- 1
2
3 659 • The channel routing outputs contain more information of simulation bias than
4
5 660 timing, meaning the channel router moves with poor timing, but conserves mass
6
7 661 well.
8
9
10 662 • The land surface outputs contain more information of simulation timing than bias,
11
12 663 meaning the land surface component does not conserve mass well, but delivers
13
14 664 water to the channel at appropriate times.
15
16
17 665 • Information is lost during channel routing after the mass is delivered, indicating
18
19 666 the channel router is not functioning properly.
20
21

22 667 There is potential to expand this analysis, breaking down the NWM components even further.
23
24 668 Quantification can be done with the full state space from the NWM. Retrospective runs using
25
26 669 new versions of the NWM should output the full state space for these types of analysis. This
27
28 670 diagnostics analysis using ML post-processing is possible with any physics-based, conceptual or
29
30 671 process-based dynamics model.
31
32

33 34 672 *Moving forward with theory-guided machine learning* 35 36

37 673 The post-processing procedure presented here is one of the cruder techniques currently
38
39 674 available for combining process-based and data-driven models. Several other methods of
40
41 675 combining the benefits of machine learning (predictability) with the benefits of physically
42
43 676 realistic hydrologic theory (robustness) are in development. For example, Pelissier *et al.* (2019)
44
45 677 integrated a trained Gaussian Processes into the state-space dynamics of a process-based land
46
47 678 surface model for predicting soil moisture time series. Another example is using physical
48
49 679 principles to constrain the loss function of an ML model during training - for example Hoedt *et*
50
51 680 *al.* (2020) integrated mass balance constraints into an LSTM and applied this model to the same
52
53 681 531 basins used in this study. Implementing post-processing is relatively straightforward
54
55
56
57
58
59
60

1
2
3 682 compared to other techniques such as adding physics into ML code or using ML to dynamically
4
5 683 update the state variables, but is unreliable when the process-based models used as input is
6
7
8 684 uncalibrated.
9

10
11 685 Using ML for post-processing has potential for advancing the explainability of data-
12
13 686 driven models. We showed that the LSTM model representation of hydrologic signatures (with
14
15 687 and without NWM model outputs) is highly correlated with the NWM. This indicates that the
16
17 688 “learned” functions mapping inputs to streamflow are actually quite similar. We might have
18
19 689 trouble expressing the “learned” LSTM with compact formulas (*e.g.*, PDEs), given the high
20
21 690 number of trained model weights, but we can use them with confidence knowing their structural
22
23 691 similarities with process-based models like the NWM.
24
25

26 27 28 692 **CONCLUSION**

29
30
31 693 The LSTM post-processors (LSTM_PPA and LSTM_PP) significantly outperformed the
32
33 694 NWM, but did not consistently, nor significantly, outperform the LSTM_A (the LSTM model
34
35 695 trained without the NWM model outputs as LSTM inputs). LSTMs, in general, are capable of
36
37 696 learning the dynamics of rainfall-runoff processes, gaining little additional information from the
38
39 697 conceptualizations coded within the NWM. The “pure” post-processing model (LSTM_PP)
40
41 698 outperformed the NWM in terms of bias, and significantly outperformed the NWM in terms of
42
43 699 NSE and timing. A decision to use the LSTM as a post-processor for the NWM should be made
44
45 700 with professional judgement, considering the comparison of the NWM, LSTM and LSTM post-
46
47 701 processor’s performance. In locations where the NWM is not calibrated, or the hydrologic
48
49 702 conditions are not well understood, it would be best to use the LSTM without the influence from
50
51 703 the NWM.
52
53
54
55
56
57
58
59
60

1
2
3 704 The results indicate that there is more information in the atmospheric forcings about
4
5 705 streamflow observations than in the NWM outputs, including the NWM streamflow prediction.
6
7
8 706 The NWM loses information between the atmospheric forcing inputs and the outputs. The NWM
9
10 707 land surface component (LDAS) loses information about mass conservation (shown from the
11
12 708 bias error), and the channel router (CHRT) loses information about streamflow timing. The
13
14
15 709 NWM routing scheme should be considered as a priority for improving the NWM.
16

710 DATA AVAILABILITY

17
18
19
20
21 711 All data and code used in this paper are publicly available in the following locations:
22
23 712 **U.S. National Water Model:** <https://docs.opendata.aws/nwm-archive/readme.html>
24
25 713 **CAMELS data:** <https://ral.ucar.edu/solutions/products/camels>
26
27 714 **Data processing code:** <https://github.com/jmframe/nwm-reanalysis-model-data-processing>,
28 715 DOI: 10.5281/zenodo.4642605
29
30 716 **LSTM code:** https://github.com/kratzert/ealstm_regional_modeling
31
32 717 **Post-processing and analysis code:** [https://github.com/jmframe/nwm-post-processing-with-](https://github.com/jmframe/nwm-post-processing-with-lstm)
33 718 [lstm](https://github.com/jmframe/nwm-post-processing-with-lstm), DOI: 10.5281/zenodo.4642603
34

35 719

36 720 ACKNOWLEDGEMENTS

37
38
39 721 Authors from Johannes Kepler University were partially supported by a Google faculty research
40
41 722 award. Jonathan Frame from the University of Alabama supported by the NASA Terrestrial
42
43 723 Hydrology Program. Grey Nearing (then at the University of Alabama) was partially supported
44
45 724 by the NCAR COMET program on a cooperative award with the National Water Center. The
46
47
48 725 LSTM models presented here were trained using computational resources from the NASA
49
50
51 726 Center for Climate Simulation. We thank the reviewers for their valuable feedback and
52
53 727 constructive criticism throughout the review of this paper.
54
55
56
57
58
59
60

1
2
3 728 **LITERATURE CITED**
4
5

- 6 729 Addor, N., A.J. Newman, N. Mizukami, and M. P. Clark, 2017. The CAMELS Data Set:
7
8 730 Catchment Attributes and Meteorology for Large-Sample Studies. *Earth Syst. Sci* 21:
9
10 731 5293–5313. <https://doi.org/10.5194/hess-21-5293-2017>.
12
13
14 732 Addor, N., G. Nearing, C. Prieto, A. J. Newman, N. Le Vine, and M. P. Clark, 2018. A
15
16 733 Ranking of Hydrological Signatures Based on Their Predictability in Space. *Water*
17
18 734 *Resources Research* 54, no. 11: 8792–8812. <https://doi.org/10.1029/2018WR022606>.
20
21 735 Chadalawada, J., H. M.V.V. Herath, and V. Babovic, 2020. Hydrologically Informed
22
23 736 Machine Learning for Rainfall-Runoff Modeling: A Genetic Programming-Based
24
25 737 Toolkit for Automatic Model Induction. *Water Resources Research* 56, no. 4: 1–23.
26
27 738 <https://doi.org/10.1029/2019WR026933>.
30
31 739 Cosgrove, B, D. Gochis, E. P. Clark, Z. Cui, A. L. Dugger, G. M. Fall, X. Feng, M. A.
32
33 740 Fresch, J. J. Gourley, S. Khan, D. Kitzmiller, H. S. Lee, Y. Liu, J. L. McCreight, A. J.
34
35 741 Newman, A. Oubeidillah, L. Pan, C. Pham, F. Salas, K. M. Sampson, M. Smith, G.
36
37 742 Sood, A. Wood, D. N. Yates, W. Yu and Y. Zhang, 2015. Hydrologic Modeling at the
38
39 743 National Water Center: Operational Implementation of the WRF-Hydro Model to
40
41 744 Support National Weather Service Hydrology. In AGU Fall Meeting Abstracts.
42
43
44
45
46 745 Daw, A., R. Q. Thomas, C. C. Carey, J. S. Read, A. P. Appling, and Anuj Karpatne, 2020.
47
48 746 Physics-Guided Architecture (PGA) of Neural Networks for Quantifying Uncertainty
49
50 747 in Lake Temperature Modeling. Proceedings of the 2020 SIAM International
51
52 748 Conference on Data Mining, 532–40. <https://doi.org/10.1137/1.9781611976236.60>.
53
54
55
56
57
58
59
60

Revised manuscript submitted to the Journal of The American Water Resources Association (JAWRA) March 2021

1
2
3 749 Elmer, N. J., 2019. Using Satellite Observations of River Height and Vegetation To Improve
4
5 750 National Water Model Initialization and Streamflow Prediction. PhD diss., The
6
7
8 751 University of Alabama in Huntsville.

9
10
11 752 Gauch, Martin, Juliane Mai, and Jimmy Lin. 2021, The Proper Care and Feeding of
12
13 753 CAMELS: How Limited Training Data Affects Streamflow Prediction. Environmental
14
15 754 Modelling and Software 135, no. November 2020 (2021): 104926.
16
17
18 755 <https://doi.org/10.1016/j.envsoft.2020.104926>.

19
20
21 756
22
23
24 757 Gauch, Martin, Frederik Kratzert, Daniel Klotz, Grey Nearing, Jimmy Lin, and Sepp
25
26 758 Hochreiter, 2021. Rainfall-Runoff Prediction at Multiple Timescales with a Single
27
28 759 Long Short-Term Memory Network. Hydrology and Earth System Sciences 25, no. 4
29
30
31 760 (2021): 2045–62. <https://doi.org/10.5194/hess-25-2045-2021>.

32
33
34 761
35
36
37 762 Gupta, H. V., T. Wagener, and Y. Liu, 2008. Reconciling Theory with Observations:
38
39 763 Elements of a Diagnostic Approach to Model Evaluation. Hydrological Processes
40
41 764 2274, no. November 2008: 2267–74. <https://doi.org/10.1002/hyp.6989>.

42
43
44 765 Gupta, H. V., H. Kling, K. K. Yilmaz, and G. F. Martinez, 2009. Decomposition of the
45
46 766 Mean Squared Error and NSE Performance Criteria: Implications for Improving
47
48
49 767 Hydrological Modelling. Journal of Hydrology 377, no. 1–2: 80–91.
50
51 768 <https://doi.org/10.1016/j.jhydrol.2009.08.003>.

- 1
2
3 769 Han, Heechan. 2021. Improving Hydrologic Modeling of Runoff Processes Using Data-
4
5 770 Driven Models. Doctoral diss., Colorado State University, 2021.
6
7 771 https://mountainscholar.org/bitstream/handle/10217/232583/Han_colostate_0053A_16
8
9 772 [465.pdf?sequence=1&isAllowed=y](https://mountainscholar.org/bitstream/handle/10217/232583/Han_colostate_0053A_16465.pdf?sequence=1&isAllowed=y).
10
11
12
13 773 Hansen, C., J. S. Shiva, S. McDonald, and A. Nabors, 2019. Assessing Retrospective
14
15 774 National Water Model Streamflow with Respect to Droughts and Low Flows in the
16
17 775 Colorado River Basin. *Journal of the American Water Resources Association* 55, no. 4:
18
19 776 964–75. <https://doi.org/10.1111/1752-1688.12784>.
20
21
22
23 777 Hochreiter, S, 1991. *Untersuchungen Zu Dynamischen Neuronalen Netzen*. Doctoral diss.,
24
25 778 Institut Für Informatik, Technische Universität, Munchen
26
27 779 <http://people.idsia.ch/~juergen/SeppHochreiter1991ThesisAdvisorSchmidhuber.pdf>.
28
29
30
31 780 Hochreiter, S., and J. Schmidhuber, 1997. Long Short-Term Memory. *Neural Computation*
32
33 781 9, no. 8: 1735–80. <https://doi.org/10.1162/neco.1997.9.8.1735>.
34
35
36 782 Hoedt, P. J., F. Kratzert, D. Klotz, C. Halmich, M. Holzleitner, G. Nearing, S. Hochreiter,
37
38 783 and G. Klambauer. 2021. MC-LSTM: Mass-Conserving LSTM, 2021, 1–32.
39
40 784 <http://arxiv.org/abs/2101.05186>.
41
42
43
44 785 Karpatne, A., W. Watkins, J. Read, and V. Kumar, 2017a. Physics-Guided Neural Networks
45
46 786 (PGNN): An Application in Lake Temperature Modeling.
47
48 787 <http://arxiv.org/abs/1710.11431>.
49
50
51 788 Karpatne, A., G. Atluri, J. H. Faghmous, M. Steinbach, A. Banerjee, A. Ganguly, S.
52
53 789 Shekhar, N. Samatova, and V. Kumar, 2017b. Theory-Guided Data Science: A New
54
55
56
57
58
59
60

Revised manuscript submitted to the Journal of The American Water Resources Association (JAWRA) March 2021

- 1
2
3 790 Paradigm for Scientific Discovery from Data. IEEE Transactions on Knowledge and
4
5 791 Data Engineering 29, no. 10: 2318–31. <https://doi.org/10.1109/TKDE.2017.2720168>.
6
7
8 792 Kim, J., L. Read, L. E. Johnson, D. Gochis, R. Cifelli, and H. Han, 2020. An Experiment on
9
10 793 Reservoir Representation Schemes to Improve Hydrologic Prediction: Coupling the
11
12 794 National Water Model with the HEC-ResSim. Hydrological Sciences Journal 0, no. 0:
13
14 795 1. <https://doi.org/10.1080/02626667.2020.1757677>.
15
16
17
18 796 Klemeš, V, 1986. Dilettantism in Hydrology: Transition or Destiny? Water Resources
19
20 797 Research 22, no. 9 S: 177S-188S. <https://doi.org/10.1029/WR022i09Sp0177S>.
21
22
23
24 798 Kratzert, F., D. Klotz, C. Brenner, K. Schulz, and M. Herrnegger, 2018. Rainfall–Runoff
25
26 799 Modelling Using Long Short-Term Memory (LSTM) Networks. Hydrology and Earth
27
28 800 System Sciences 22, no. 11: 6005–22. <https://doi.org/10.5194/hess-22-6005-2018>.
29
30
31 801 Kratzert, F., D. Klotz, M. Herrnegger, A. K. Sampson, S. Hochreiter, and G. S. Nearing,
32
33 802 2019a. Towards Improved Predictions in Ungauged Basins: Exploiting the Power of
34
35 803 Machine Learning. Water Resources Research, 2019WR026065.
36
37 804 <https://doi.org/10.1029/2019WR026065>.
38
39
40
41 805 Kratzert, F., D. Klotz, G. Shalev, G. Klambauer, S. Hochreiter, and G. S. Nearing, 2019b.
42
43 806 Towards Learning Universal, Regional, and Local Hydrological Behaviors via
44
45 807 Machine Learning Applied to Large-Sample Datasets. Hydrology and Earth System
46
47 808 Sciences 23, no. 12: 5089–5110. <https://doi.org/10.5194/hess-23-5089-2019>.
48
49
50
51 809 Nearing, G. S., Benjamin L. Ruddell, Martyn P. Clark, Bart Nijssen, and Christa Peters-
52
53 810 Lidard. “Benchmarking and Process Diagnostics of Land Models.” Journal of
54
55
56
57
58
59
60

- 1
2
3 811 Hydrometeorology, 2018, JHM-D-17-0209.1. [https://doi.org/10.1175/JHM-D-17-](https://doi.org/10.1175/JHM-D-17-0209.1)
4
5 812 [0209.1](https://doi.org/10.1175/JHM-D-17-0209.1).
6
7
8 813 Nearing, G. S., F. Kratzert, D. Klotz, P.J. Hoedt, G. Klambauer, S. Hochreiter, H. Gupta, S.
9
10 814 Nevo, and Y. Matias. 2020. A Deep Learning Architecture for Conservative
11
12 815 Dynamical Systems: Application to Rainfall-Runoff Modeling. AI for Earth Sciences
13
14 816 Workshop at NEURIPS 2020, 2020.
- 17
18 817 Newman, A. J., M. P. Clark, K. Sampson, A. Wood, L. E. Hay, A. Bock, R. J. Viger, D.
19
20 818 Blodgett, L. Brekke, J. R. Arnold, T. Hopson, and Q. Duan, 2015. Development of a
21
22 819 Large-Sample Watershed-Scale Hydrometeorological Data Set for the Contiguous
23
24 820 USA: Data Set Characteristics and Assessment of Regional Variability in Hydrologic
25
26 821 Model Performance. Hydrology and Earth System Sciences 19, no. 1: 209–23.
27
28 822 <https://doi.org/10.5194/hess-19-209-2015>.
29
30
31
32
33 823 Niu, G.-Y., et al. (2011), The community Noah land surface model with
34
35 824 multiparameterization options (Noah-MP): 1. Model description and evaluation with
36
37 825 local-scale measurements. J. Geophys. Res., 116, D12109, doi:
38
39 826 10.1029/2010JD015139.
- 41
42
43 827 National Oceanic and Atmospheric Administration (NOAA). 2019. Stakeholder
44
45 828 Engagement to Inform National Weather Service Hydrologic Products and Services to
46
47 829 Meet User Needs NOAA National Weather Service Water Resources Services Branch
48
49
50 830 and Office of Water Prediction.
51
52 831 [https://www.weather.gov/media/water/StakeholderEngagementtoInformNWMProducts](https://www.weather.gov/media/water/StakeholderEngagementtoInformNWMProductsServices2019.pdf)
53
54 832 [Services2019.pdf](https://www.weather.gov/media/water/StakeholderEngagementtoInformNWMProductsServices2019.pdf)
55
56
57
58
59
60

Revised manuscript submitted to the Journal of The American Water Resources Association (JAWRA) March 2021

- 1
2
3 833 Pelissier, C., J. Frame, and G. Nearing, 2019. Combining Parametric Land Surface Models
4
5 834 with Machine Learning. arXiv preprint arXiv:2002.06141.
6
7
8 835 Read, J. S., Jia, X., Willard, J., Appling, A. P., Zwart, J. A., Oliver, S. K., et al. 2019.
9
10 836 Process-guided deep learning predictions of lake water temperature. *Water Resources*
11
12 837 *Research*, 55, 9173– 9190. <https://doi.org/10.1029/2019WR024922>
13
14
15
16 838 Reichstein, M., G. Camps-valls, B. Stevens, M. Jung, J. Denzler, and N. Carvalhais, 2019.
17
18 839 Deep Learning and Process Understanding for Data-Driven Earth System Science.
19
20 840 *Nature* 566: 195–204. <https://doi.org/10.1038/s41586-019-0912-1>.
21
22
23
24 841 Salas, F. R., M. A. Somos-Valenzuela, A. Dugger, D. R. Maidment, D. J. Gochis, C. H.
25
26 842 David, W. Yu, D. Ding, E. P. Clark, and N. Noman, 2018. Towards Real-Time
27
28 843 Continental Scale Streamflow Simulation in Continuous and Discrete Space. *Journal of*
29
30 844 *the American Water Resources Association* 54, no. 1: 7–27.
31
32 845 <https://doi.org/10.1111/1752-1688.12586>.
33
34
35
36 846 Steiger, J., and M. Browne, 1984. The Comparison of Interdependent Correlations between
37
38 847 Optimal Linear Composites. *Psychometrika* 49, no. 1: 11–24.
39
40 848 <https://doi.org/10.1017/CBO9781107415324.004>.
41
42
43
44 849 Sundararajan, M., A. Taly, and Q. Yan, 2017. Axiomatic Attribution for Deep Networks.
45
46 850 34th International Conference on Machine Learning, ICML 2017 7: 5109–18.
47
48
49 851 Tartakovsky, A. M., C. O. Marrero, P. Perdikaris, G. D. Tartakovsky, and D. Barajas-
50
51 852 Solano, 2020. Physics-Informed Deep Neural Networks for Learning Parameters and
52
53 853 Constitutive Relationships in Subsurface Flow Problems. *Water Resources Research*
54
55 854 56, no. 5: 1–16. <https://doi.org/10.1029/2019WR026731>.
56
57
58
59
60

1
2
3 855 Xia, Y., K. Mitchell, M. Ek, J. Sheffield, B. Cosgrove, E. Wood, L. Luo, C. Alonge, H.
4
5 856 Wei, J. Meng, B. Livneh, D. Lettenmaier, V. Koren, Q. Duan, K. Mo, Y. Fan, and D.
6
7 857 Mocko, 2012. Continental-Scale Water and Energy Flux Analysis and Validation for
8
9 the North American Land Data Assimilation System Project Phase 2 (NLDAS-2): 1.
10 858
11 Intercomparison and Application of Model Products. Journal of Geophysical Research
12 859
13 Atmospheres 117, no. 3. <https://doi.org/10.1029/2011JD016048>.
14 860
15
16
17 861 Ye, A., Q. Duan, X. Yuan, E. F Wood, and J. Schaake, 2014. Hydrologic Post-Processing
18
19 of MOPEX Streamflow Simulations. Journal of Hydrology 508: 147–56.
20 862
21
22 863 <https://doi.org/10.1016/j.jhydrol.2013.10.055>.
23
24
25
26
27
28
29
30
31
32
33
34
35
36
37
38
39
40
41
42
43
44
45
46
47
48
49
50
51
52
53
54
55
56
57
58
59
60